UNIVERSITÉ DU QUÉBEC À TROIS-RIVIÈRES

RECONSTRUCTION ET ANALYSE DE SENSIBILITÉ CLIMATIQUE DU BILAN DE MASSE DU GLACIER SASKATCHEWAN, CANADA

MÉMOIRE PRÉSENTÉ
COMME EXIGENCE PARTIELLE DE LA
MAÎTRISE EN SCIENCES DE L'ENVIRONNEMENT

PAR
OLIVIER LAROUCHE

AVRIL 2020

Université du Québec à Trois-Rivières

Service de la bibliothèque

Avertissement

L'auteur de ce mémoire ou de cette thèse a autorisé l'Université du Québec à Trois-Rivières à diffuser, à des fins non lucratives, une copie de son mémoire ou de sa thèse.

Cette diffusion n'entraîne pas une renonciation de la part de l'auteur à ses droits de propriété intellectuelle, incluant le droit d'auteur, sur ce mémoire ou cette thèse. Notamment, la reproduction ou la publication de la totalité ou d'une partie importante de ce mémoire ou de cette thèse requiert son autorisation.

REMERCIEMENTS

L'information contenue dans ce mémoire est le résultat de quatre ans d'efforts soutenus parallèlement à mes nombreuses autres passions. Ce cheminement m'a fait développer de nouvelles connaissances et expertises, tant dans les sciences de l'environnement que dans la gestion de projet. Cette expérience m'a permis d'évoluer grandement sur le plan personnel et de faire des rencontres de gens extraordinaires tout au long de mon parcours : des gens qui ont à cœur le bon fonctionnement de la planète et de ses écosystèmes.

Je tiens à remercier mon directeur de maîtrise M. Christophe Kinnard, professeur du Département des sciences de l'environnement de l'Université du Québec à Trois-Rivières, de m'avoir fait confiance pour ce projet ambitieux. Il a fait part d'une grande disponibilité, d'optimisme et d'efficacité tout au long de la recherche.

Je tiens également à remercier les membres du jury qui ont accepté d'évaluer mon travail : MM. Denis Gratton et Ali Assani, professeurs du Département des sciences de l'environnement de l'Université du Québec à Trois-Rivières. Merci à Michael Demuth, de la Commission géologique du Canada, de nous avoir permis de réaliser les travaux de recherche sur le champ de glace Columbia.

Je remercie tous les gens qui sont passés et qui travaillent actuellement au Laboratoire en environnement des régions froides (GLACIOLAB) : Okan Aygün, Hafsa Bouamri, Vasana Sandamali Dharmadasa, Hadi Mohammadzadeh Khani, Ghada Bzeouich, Matthieu Loyer, Gabriel Meunier Cardinal, Saida Nemri, Anthony Pothier Champagne, Lisane Arseneault, Arthur de Grandpré et les autres.

Finalement, merci à ma famille et mes amis qui m'ont soutenu tout au long de mon parcours, mais surtout à ma conjointe Amélie qui m'a redonné le sourire chaque fois que j'en ai eu besoin.

RÉSUMÉ

Sur les sites où les observations de bilan de masse à long terme sont rares, des modèles sont nécessaires pour la reconstitution du bilan de masse historique des glaciers et pour l'évaluation de sa sensibilité au changement climatique. Dans cette étude, nous avons utilisé le produit d'assimilation de données North American Regional Reanalysis (NARR) avec une résolution spatiale de 32 × 32 km et une résolution temporelle de 3 heures pour produire les forçages météorologiques nécessaires à l'élaboration d'un modèle de bilan de masse distribué et physique du glacier Saskatchewan (DEBAM) pendant la période historique 1979-2016. Un enregistrement de deux ans (2014-2016) d'une station météorologique automatique sur le glacier (AWS) et un enregistrement historique homogénéisé des précipitations de deux stations météorologiques permanentes voisines ont été utilisées pour mettre à l'échelle la température de l'air, l'humidité relative, la vitesse du vent, le rayonnement solaire entrant et les précipitations du point de grille NARR le plus près de l'AWS du glacier Saskatchewan. Le modèle a été appliqué avec une géométrie fixe (1979) et variable dans le temps à l'aide d'un ensemble de données de modèle numérique d'élévation (DEM) multi temporel publié précédemment (1979, 1986, 1993, 2001 et 2009). Le modèle a été validé à partir d'observations glaciologiques récentes du bilan de masse et a montré une bonne performance (ba : NSE = 0,94). La comparaison entre le bilan de masse cumulatif reconstitué et les estimations du bilan de masse géodésique publiées antérieurement a montré une concordance raisonnable. La différence entre les simulations statiques et dynamiques a montré peu de différence (1,4 m d'équivalent en eau (w.e.) sur 37 ans), ce qui suggère que le recul du glacier n'a pas encore eu un impact important sur le bilan de masse spécifique. Le modèle a été utilisé pour évaluer la sensibilité du bilan de masse statique aux changements prescrits de la température moyenne régionale de l'air entre 0 et 8 °C et des précipitations entre -20 et +20 %, ce qui comprend les scénarios RCP du GIEC +2,6, +4,5, +6,0 et +8,5 Wm^{-2} pour le milieu (2046-2065) et la fin (2081-2100) du XXI^{e} siècle. Le bilan de masse annuel moyen historique modélisé était de -0,49 m w.e. a^{-1} et pourrait augmenter jusqu'à -3 m w.e. a^{-1} d'ici la fin du siècle en réponse à un réchauffement de la température de l'air de +3 °C et à une augmentation de 8 % des précipitations, pour le scénario RCP +6.0. En conclusion, même avec des observations de terrain restreintes, le forçage d'un modèle à bilan d'énergie basé sur les processus physiques par des réanalyses climatiques permet d'obtenir des informations importantes sur le bilan de masse passé et futur de glaciers mal échantillonnés comme le glacier de la Saskatchewan.

Mots-clés : modélisation physique du bilan de masse glaciaire, bilan d'énergie, réanalyses climatiques NARR, sensibilité climatique, glacier Saskatchewan, champs de glace Columbia, Canada.

TABLE DES MATIÈRES

CHAPITRE I

INTRODUCTION

1.1 Mise en contexte

Les glaciers représentent 69 % de la réserve mondiale en eau douce, ce qui en fait un intérêt majeur pour l'humanité (Shiklomanov, 1998). Toutefois, l'accessibilité à cette ressource n'est pas toujours possible, car la majorité des glaciers se retrouvent dans des endroits isolés. Un impressionnant jeu de données est recueilli depuis plus d'un siècle à travers le monde par le *World Glacier Monitoring Service* (WGMS), une organisation qui se penche sur l'étude des glaciers de tous les continents. Ces observations incluent le bilan de masse glaciologique et les changements morphologiques de nombreux glaciers et permettent de constater que pratiquement tous les glaciers sont en perte de masse depuis la fin du Petit âge glaciaire (Oerlemans, 1994; Zemp et al., 2015), une période climatique froide qui a permis l'expansion de la majorité des glaciers de l'hémisphère Nord dès le 14^{e} siècle jusqu'à la fin du 19^{e} siècle (Matthews et Briffa, 2005).

Les glaciers se forment aux endroits où les conditions climatiques et topographiques permettent l'accumulation et la préservation de la neige. Le bilan de masse représente la différence entre l'accumulation de neige (gains) et l'ablation de la glace (pertes) au cours d'une année. Une accumulation importante de neige en hiver et une ablation faible en été favoriseront un bilan de masse annuel positif causant une expansion du glacier à plus long terme, et vice-versa. Les glaciers sont ainsi de bons indicateurs climatiques en raison de leur réponse directe au bilan de masse et aux variations de température et précipitations, en fonction de la topographie environnante (Benn et Evans, 2010, p. 48).

Les variations du bilan de masse des glaciers sont intimement liées au cycle régional de l'eau (Zemp et al., 2015) et au niveau des océans (Marzeion et al., 2012). L'eau, sous l'état gazeux, liquide et solide, est constamment en évolution, transitant depuis

l'océan vers l'atmosphère, puis de la cryosphère vers l'hydrosphère. Les variations du climat modifient ainsi la quantité d'eau stockée sous forme solide sur les continents (Benn et Evans, 2010, p. 5). Les glaciers agissent aussi comme régulateurs au sein d'un bassin versant en stockant de l'eau qui est progressivement réintroduite dans le système sur une base allant de saisonnière à interannuelle (Jansson et al., 2003).

L'eau de fonte de la neige accumulée en hiver est libérée progressivement au printemps, alors que la fonte de la glace se poursuit tout l'été : les débits hydrologiques des bassins englacés sont ainsi plus élevés à la fin de l'été comparativement aux bassins non englacés. Les utilisateurs de la ressource peuvent ainsi bénéficier d'un débit constant durant une période où le niveau d'eau serait autrement plus faible en raison de l'amenuisement des stocks de neige et des précipitations plus faibles en été. Les glaciers agissent ainsi comme zones tampons sur le cycle hydrologique (Comeau et al., 2009).

Les montagnes sont indispensables dans le système planétaire. Elles occupent près de 25 % de la superficie des continents (Kapos et al., 2000) et sont une importante source d'eau douce, d'énergie, de minerais et de forêt. Le tourisme y est fleurissant et les zones agricoles s'y retrouvent en grand nombre dans les vallées (Beniston, 2003). Bien que seulement 26 % de la population réside dans les montagnes ou au pied de celles-ci (Meybeck et al., 2001), plus de 40 % de la population globale réside dans les bassins versants de rivières approvisionnées par les montagnes (Beniston, 2003). Au Canada, les Prairies sont alimentées en bonne partie par la neige et les glaciers accumulés dans les montagnes Rocheuses à l'Ouest. Des travaux récents prédisent une déglaciation progressive des montagnes Rocheuses au cours du prochain siècle, ce qui menace la contribution hydrologique des glaciers à long terme (Clarke et al., 2015). L'agriculture (Barnett et al., 2005; Schindler et Donahue, 2006; Comeau et al., 2009) et les pêcheries en eau douce (Dittmer, 2013; Grah et Beaulieu, 2013) d'une bonne partie du pays pourraient donc être affectées par la perte progressive des surfaces glaciaires et neigeuses en réponse au réchauffement climatique. Un réchauffement climatique induirait moins de précipitations neigeuses dans les régions froides, une fonte plus hâtive de la neige au printemps et une période plus longue de fonte de la glace en été. Même si la quantité de

précipitations ne diminuait pas, la capacité de stockage de l'eau serait moins efficace puisqu'elle serait perdue plus rapidement vers l'océan (Barnett et al., 2005). En excluant les grands inlandsis (Groenland et Antarctique), les glaciers ont contribué à l'augmentation du niveau marin de 114 ± 5 mm entre 1902 et 2009 (Marzeion et al., 2012) et 1,48 ± 0,26 mm par année entre 2003 à 2010 (Jacob et al., 2012). Des projections estiment une augmentation d'entre 155 ± 41 mm (Radić et al., 2014) et 166 ± 44 mm (Marzeion et al., 2012) du niveau marin en 2100 selon le scénario RCP 4.5, ce qui submergerait une bonne partie des côtes océaniques et forcerait le mouvement des populations (Meier et al., 2007; Nicholls et Cazenave, 2010).

1.2 Problématique

Un grand nombre d'études ont démontré un retrait quasi généralisé des glaciers dans le monde depuis la seconde moitié du 19^{e} siècle (Kaser, 1999; Zemp et al., 2015; Barry, 2006). Dans les Rocheuses canadiennes, Bolch et al. (2010) ont comparé des images satellitaires de 1985 à 2005 et ont rapporté une diminution de 11 % (± 4 %) de la surface des glaciers de l'Ouest canadien (Bolch et al., 2010). Sur la période de 1919-2006, une étude plus récente rapporte une diminution de 30 % de la surface des glaciers, soit 750 km^2 dans le centre et le sud des Rocheuses canadiennes (Tennant et al., 2012). Selon des travaux de modélisation plus récents, le volume des glaciers du Canada pourrait diminuer de 70 % (± 10 %) de 2005 à 2100, et de 90 % dans les Rocheuses canadiennes (Clarke et al., 2015).

Considérant le glacier comme un système, le bilan de masse glaciologique correspond à la différence entre le volume d'eau accumulée sous forme de glace ou de neige et le volume d'eau perdu, sur une période donnée (Cuffey et Paterson, 2010, p. 128). Les facteurs à prendre en considération pour la mesure et le calcul du bilan de masse glaciologique se séparent en deux groupes : météorologiques et topographiques. La récolte de l'information météorologique se fait à l'aide de stations automatisées sur ou près du glacier. Des balises d'ablation peuvent être installées à plusieurs endroits au centre du glacier pour mesurer la perte et le gain de masse. Des capteurs de température et

d'humidité peuvent également être fixés sur ces balises pour mesurer les écarts thermiques entre le sommet et la vallée du glacier. De plus, l'utilisation d'images satellitaires à faible résolution spatiale permet de calculer la surface du glacier de façon régulière, afin d'y extrapoler les mesures ponctuelles réalisées sur le terrain. La prise de photographies aériennes de basse altitude ainsi qu'un travail de reconstruction photogrammétrique permettent de dériver la topographie de la surface glaciaire (Digital Elevation Model : DEM). Le bilan de masse glaciologique peut être ainsi estimé en différenciant ces surfaces topographiques dans le temps. En raison des coûts et des difficultés logistiques liées aux mesures du bilan de masse sur le terrain, peu de sites détiennent ces données sur de longues périodes.

Étant donné la difficulté d'acquérir de l'information, la projection de l'impact des changements climatiques sur les glaciers nécessite l'élaboration et l'application de modèles de bilan de masse glaciologique. Cette approche repose sur l'estimation du climat d'un bassin glaciaire sur une période donnée à partir de données météorologiques et topographiques. Plusieurs types de modèles existent et leur complexité varie grandement en fonction des processus représentés, des données requises en entrée et de la résolution spatiale et temporelle du modèle. La majorité des travaux portant sur l'impact des changements climatiques sur les glaciers ont utilisé des modèles empiriques basés uniquement sur la température de l'air et les précipitations, en raison de leur simplicité d'application et de la disponibilité de l'information. Cette approche est connue sous le nom de modèle « degrés-jours » (en anglais : « Temperature-index (TI) » ou « Degree-days » model) (Hock, 2003; Pellicciotti et al., 2005; Carenzo et al., 2009; Matthews et al., 2015). Ces modèles simples contiennent peu de paramètres, ce qui facilite leur application, mais ceux-ci doivent être calibrés sur des observations. L'extrapolation des paramètres dans le temps et dans l'espace, c'est-à-dire en dehors des conditions de calibration, est donc discutable (Hock, 2003; Carenzo et al., 2009; Wheler, 2009). D'autre part, les modèles à base physique, dont le calcul de l'ablation repose sur la résolution du bilan d'énergie en surface du glacier (en anglais « Energy-balance (EB) » model), sont plus complexes puisqu'ils contiennent plusieurs paramètres qui ne sont pas toujours faciles à estimer et, de manière générale, requièrent plusieurs types de données en entrée (Hock et Holmgren,

2005; Carenzo, 2012). Ces modèles sont toutefois considérés plus fiables pour simuler l'impact des changements climatiques, à condition de disposer des données requises. Des modèles de « complexité intermédiaire » ou « améliorés » (en anglais « Enhanced Temperature-Index (ETI) » model) (Hock, 1999; Pellicciotti et al., 2005) sont à base empirique, mais incluent davantage de processus physiques. Ils ont été développés pour combler les lacunes des deux méthodes principales (TI et EB).

Les modèles empiriques tirent leur force de leur simplicité d'application et du peu de données requise en entrée, ce qui les rend pratiques pour simuler la réponse des glaciers au climat à l'échelle d'un massif montagneux (Hock, 2003; Marshall et al., 2011; Immerzeel et al., 2013; Radić et al., 2014; Clarke et al., 2015) et même global (Raper et Braithwaite, 2006; Marzeion et al., 2012; Radić et al., 2014). Cependant, ces modèles simples sont plus susceptibles de contenir des erreurs structurelles, c'est-à-dire de souffrir d'un manque de représentativité physique (Hock et Radić, 2007), que les modèles à base physique. La calibration de ces modèles sur des observations a ainsi comme effet de minimiser à la fois les erreurs d'observations et les erreurs structurelles du modèle. Les paramètres calibrés sont donc optimaux pour la période de calibration, mais ne sont pas nécessairement transférables en dehors de la période et du site de calibration (Carenzo et al., 2009). Les modèles physiques, pour leur part, sont difficilement applicables à grande échelle en raison de la grande quantité de paramètres à définir et des multiples données météorologiques requises et souvent indisponibles (MacDougall et Flowers, 2011). Même si ces modèles ont le potentiel de bien simuler l'état du système glaciologique, leur application à grande échelle est encore restreinte.

Sur les sites pour lesquels les données sont rares ou manquantes, les résultats des modèles de prévision météorologique (Mölg et al., 2012; Radic et al., 2018; Bonekamp et al., 2019) et les données de réanalyse à échelle réduite (Radić et Hock, 2006; Hofer et al., 2010; Clarke et al., 2015; Østby et al., 2017) ont été utilisés pour forcer des modèles à base physiques. Les réanalyses climatiques fournissent des estimations cohérentes et robustes de l'état de l'atmosphère sur de longues périodes historiques, en s'appuyant sur l'assimilation d'observations à long terme et de qualité contrôlée pour simuler les variables

atmosphériques et de surface avec une résolution de 3 h et plus. L'analyse est réalisée régulièrement, ce qui permet d'obtenir une donnée pratiquement en temps réel (Hofer et al., 2010). Les réanalyses offrent donc des alternatives prometteuses pour forcer des modèles glaciologiques et hydrologiques dans des régions où les données sont rares. Des produits régionaux comme la North American Regional Reanalysis (NARR) ont été notamment développés pour améliorer la résolution spatiale et temporelle des réanalyses à l'échelle continentale (Mesinger et al., 2006).

Plusieurs études ont évalué l'impact des changements climatiques projetés à l'échelle d'un glacier (Radić et Hock, 2006; Huss et al., 2008), d'une chaîne de montagnes (Marshall et al., 2011; Immerzeel et al., 2013; Radić et al., 2014; Clarke et al., 2015) et même globale (Raper et Braithwaite, 2006; Marzeion et al., 2012; Radić et al., 2014). La majorité de ces études ont été réalisées à l'aide de modèles empiriques simples, particulièrement pour les études à l'échelle globale, car les données pour forcer des modèles plus complexes à cette échelle ne sont pas disponibles. Suite à l'analyse de performance menée par Gabbi et al. (2014), nous sommes en mesure de nous questionner sur la validité de ces résultats. Certaines études (Giesen et Oerlemans, 2013; Huss et al., 2014) remettent en question les projections des modèles empiriques puisque leur réponse au climat est immédiate. Refsgaard et al. (2014) expose la problématique générale de la simulation environnementale par des modèles empiriques pour un climat futur. Selon ces auteurs, les changements climatiques amènent des incertitudes sur les projections des modèles environnementaux, puisque le climat sera significativement différent des conditions actuelles et historiques. Il est donc impossible de valider la performance des projections de modèles sans avoir des observations qui reflètent les conditions climatiques futures.

1.3 Objectifs

L'objectif général de ce projet de recherche est d'estimer le bilan de masse historique du glacier Saskatchewan dans les Rocheuses canadiennes et d'évaluer l'impact des changements climatiques à moyen et à long terme sur le bilan de masse glaciaire.

Cette étude permet notamment d'analyser des glaciers qui ont très peu d'observations glaciologiques et météorologiques. Les objectifs spécifiques suivants ont tous été abordés dans le chapitre II du mémoire :

1) Reconstruire le bilan de masse historique (1979-2016) du glacier Saskatchewan en forçant un modèle de bilan de masse à base physique avec des réanalyses climatiques mises à l'échelle. La question qui sous-tend cet objectif est la suivante : est-il possible de bien simuler le bilan de masse historique d'un glacier à l'aide d'un modèle glaciologique à base physique avec peu d'observations? Notre hypothèse est que le modèle glaciologique à base physique (DEBAM) forcé par les réanalyses climatiques (NARR) mise à l'échelle permet de bien simuler le bilan de masse historique du glacier Saskatchewan.

2) Analyser l'importance du retrait glaciaire (évolution de la surface entre 1979 et 2009) sur le bilan de masse spécifique du glacier. L'utilisation de plusieurs modèles numériques d'élévation (MNT) pour la simulation du bilan de masse permet de connaître la contribution du changement de la surface au bilan de masse par rapport à des simulations statiques (superficie fixe dans le temps : 1979 et 2009). La question qui sous-tend cet objectif est la suivante : est-ce que la contribution du changement de surface est importante à long terme sur le bilan de masse? Notre hypothèse propose que l'effet dynamique du glacier a un impact mineur sur le bilan de masse spécifique du glacier Saskatchewan.

3) Analyser la sensibilité du bilan de masse glaciologique à une gamme plausible de changements de températures et de précipitations, guidés par les scénarios *Representative Concentration Pathway* (RCP) établis par le Groupe d'experts intergouvernemental sur l'évolution du climat (GIEC). Ces changements climatiques sont inévitables dans une perspective à moyen (2046-2065) et long terme (2081-2100) mais de grandes incertitudes demeurent quant au scénario qui prédominera au cours des prochaines décennies, en fonction des actions entreprises pour limiter le réchauffement. La question qui sous-tend cet objectif est la suivante : est-ce que la hausse des précipitations proposée par les scénarios

RCP est en mesure de combler la perte de bilan de masse liée par la hausse des températures? Notre hypothèse est que la hausse des précipitations est trop faible pour contrer la hausse des températures.

CHAPITRE II

MASS BALANCE MODELLING AND CLIMATE SENSITIVITY OF SASKATCHEWAN GLACIER, CANADA

Article en préparation pour une soumission au journal scientifique *The Cryosphere*.

Olivier Larouche[1], Christophe Kinnard[1], Michael Demuth[2]

[1] Département des Sciences de l'environnement, Université du Québec à Trois-Rivières, Trois-Rivières, QC, Canada

[2] Commission géologique du Canada, Ottawa, ON, Canada

Corresponding author: Christophe Kinnard

E-mail: Christophe.Kinnard@uqtr.ca

Abstract

At sites with scarce long-term mass balance observations, models are needed to reconstruct past glacier mass balance and to assess its sensitivity to climate change. In this study we used data from the North American Regional Reanalysis (NARR) project with a 32 × 32 km spatial resolution and 3-hour temporal resolution to produce the meteorological forcings needed to drive a physically-based, distributed glacier mass balance model (DEBAM) of Saskatchewan Glacier for the historical period 1979-2016. A two-year record (2014-2016) from an on-glacier automatic weather station (AWS) and an homogenized historical precipitation record from two nearby permanent weather stations were used to downscale air temperature, relative humidity, wind speed, incoming solar radiation and precipitation from the nearest NARR gridpoint to the glacier AWS site. The model was run with fixed (1979) and time-varying geometry using a previously published multi-temporal digital elevation model (DEM) dataset (1979, 1986, 1993, 2001, 2009). The model was validated using recent glaciological mass balance observations and showed a good performance (ba: NSE = 0.94). Comparison between reconstructed cumulative mass balance and previously published geodetic mass balance estimates showed a reasonable agreement. The difference between the static and dynamic simulations showed little difference (1.4 m w.e. over 37 yrs), which suggests that glacier retreat has not yet impacted greatly the specific mass balance. The model was used to assess the static mass balance sensitivity to prescribed changes in regional mean air temperature between 0 to 8 °C and precipitation between -20 to +20%, which comprises IPCC representative concentration pathways (RCP) scenarios +2.6, +4.5, +6.0 and +8.5 Wm^{-2} for the mid (2046-2065) and late (2081-2100) 21st century. The modelled historical mean annual mass balance was -0.49 m w.e. a^{-1} and could increase up to -3 m w.e. a^{-1} by the end of the century in response to a +3 °C air temperature warming and a 8% increase in precipitation, for the intermediate-high RCP scenario 6.0. We conclude that even with restricted field observations, careful application of a physically-based mass balance model allows gaining important insights of past and future mass balance for poorly sampled glaciers such as Saskatchewan Glacier.

Keywords: glacier mass balance, energy balance model, calibration, mass balance reconstruction, climate change, IPCC RCP, sensitivity analysis, Saskatchewan Glacier, Columbia Icefields, Canada.

Introduction

Mountain glaciers provide important ecosystem services to population worldwide (Huss et al., 2017; Milner et al., 2017; Dittmer, 2013; Comeau et al., 2009; Barnett et al., 2005). They act as natural reservoirs which contribute fresh water during periods of drought, and as such buffer the hydrological regimes of rivers against extreme climate variability (Jansson et al., 2003; Fountain and Tangborn, 1985). Global warming is expected to cause reduced snowfall in cold regions, earlier snowmelt in spring and a longer ice melt period in summer (Barnett et al., 2005). Even if the amount of precipitation remains unchanged, warming alone will reduce snow and ice storage in catchments, profoundly affecting the seasonality of river streamflow regimes and accelerating water losses to the ocean (Barnett et al., 2005; Huss et al., 2017). Compared to glacier and snow-fed rivers, rain-fed rivers are characterized by a more variable flow rate that can lead to a succession of extreme hydrological events such as floods and droughts. The transition from nivo-glacial to more pluvial river regime would change the timing and magnitude of floods, leading to altered patterns of erosion and sediment deposition, which will affect biodiversity and water quality (Déry et al., 2009; Huss et al., 2017). Also, glaciers outside Greenland and Antarctica have contributed to sea level rise between 0.41 ± 0.08 mm a^{-1} (Jacob et al., 2012) and 0.71 ± 0.08 mm a^{-1} (Gardner et al., 2013) per year from 2003 to 2009. Including Greenland and Antarctica, it rose by 1.13 ± 0.17 mm a^{-1} between 2002 to 2006 and by 1.85 ± 0.13 mm a^{-1} between 2012 to 2016 (Bamber et al., 2018). A projected increase of 124 ± 37 mm sea-level equivalent from mountain glaciers and ice caps is estimated between 2001 to the end of the 21st century based on mid-range greenhouse emission scenario of temperature and precipitation (Radić and Hock, 2011). Glacier contribution to sea level rise will thus exacerbate coastal inundations and force population movement in several areas of the world (Meier et al., 2007; Nicholls and Cazenave, 2010). The impacts of the progressive loss of ice and snow surfaces and resulting alterations of the hydrological cycle can reach well beyond the glacierized catchments, affecting agriculture (Milner et al., 2017; Comeau et al., 2009; Barnett et al., 2005; Schindler and Donahue, 2006), fisheries (Huss et al., 2017; Dittmer, 2013; Grah and Beaulieu, 2013), hydropower and general ecological integrity (water quality, biodiversity, etc.) (Huss et al., 2017).

The state of glaciers is typically assessed by measuring their surface mass balance, which represents the difference between snow accumulation (gains) and ice ablation (losses) over the year and represents the glacier's direct response to climatic variations. It is thus the prime variable of interest to monitor and project the state of glaciers and their hydrological contribution under global warming scenarios. Prolonged periods of reduced snow accumulation in winter and/or high ablation in summer cause a negative annual mass balance, which cause the glacier to shrink on a long term. Glaciers are thus good climatic indicators because of the direct response of mass balance to temperature and precipitation variations, while glacier front variations represent delayed response to climate (Oerlemans, 2001). An impressive dataset has been collected for more than a century by the World Glacier Monitoring Service (WGMS) around the world. These observations include the glacial mass balance and morphological changes of many glaciers around the world and show that almost all glaciers are losing mass since the end of the Little Ice Age (Zemp et al., 2015; Oerlemans, 1994).

Only few glaciers around the world have long term direct mass balance observations available because these measurements are time consuming and logistically complicated. For this reason, models are often used to extrapolate scarce measurements, estimate unsampled glaciers and to assess glacier mass balance sensitivity to climate. Several types of models can be used to estimate glacier mass balance, and their complexity varies depending on the processes involved, the input data required and the spatial and temporal resolution of the models. Most studies dealing with projecting climate change impacts on glaciers relied on empirical models based mainly on air temperature and precipitation, known as 'temperature-index' or 'degree-days' models, as they are simple to implement and the forcing data is widely and readily available (Hock, 2003; Pellicciotti et al., 2005; Carenzo et al., 2009; Matthews et al., 2015). These simple models contain few parameters, which simplifies their application, but they must be calibrated on observations. The extrapolation of parameters in time and space, i.e. outside the calibration conditions, is therefore questionable (Gabbi et al., 2014; Carenzo et al., 2009; Wheler, 2009; Hock, 2003). On the other hand, physically based models rely on energy-balance calculations to explicitly account for all energy exchanges between the glacier surface and atmosphere.

They are more complex and contain several parameters that are sometimes difficult to estimate and require several input observations (Arnold et al., 1996; Klok and Oerlemans, 2002; Gerbaux et al., 2005; Mölg et al., 2008). However, these models better represent the physical processes which drive glacier ablation and can thus be used to estimate mass balance sensitivity to climate outside the present-day climate conditions. So-called 'enhanced' temperature-index models include additional predictors to air temperature, such as potential (Pellicciotti et al., 2005; Hock, 1999) or net (Pellicciotti et al., 2005) solar radiation to estimate melt. They offer a useful trade-off between the simple temperature-index models and the more complex energy-balance models and have been shown to be more transferable outside their calibration interval (Réveillet et al., 2017b; Gabbi et al., 2014; Carenzo, 2012). However, they still depend on the availability of sufficient mass balance observations for accurate calibration.

Glaciological models have been mostly forced with observations from automatic meteorological stations (AWS) on or near the glacier. However, the management of weather stations networks in mountainous areas poses financial and logistical challenges. At sites with scarce or missing data, outputs from meteorological forecasting models (Bonekamp et al., 2019; Radic et al., 2018; Mölg et al., 2012) and downscaled reanalysis data (Østby et al., 2017; Clarke et al., 2015; Hofer et al., 2010; Radić and Hock, 2006) have been used to force physically-based model. Reanalyses are produced by retrospective numerical weather model simulations which assimilate long-term and quality-controlled observations and provide consistent gridded estimates of past atmospheric states at sub-daily intervals and updated in near-real time. Reanalyses thus offer promising alternatives to drive glaciological and hydrological in data-scarce regions (Hofer et al., 2010). Regional products like the North American Regional Reanalysis (NARR) were developed to enhance the spatial and temporal resolution of reanalyses at the continental scale (Mesinger et al., 2006). However, weather station observations are normally acquired at an hourly interval while reanalysis data are produced at longer time intervals (3 to12 h) and at coarser spatial resolution (32 km^2 and more). Downscaling reanalysis data with meteorological observations allows reducing biases resulting from this temporal and spatial scale mismatch as well as from structural and parameterizations errors in the

reanalysis model (Hofer et al., 2010). The validation of the reanalysis data against the ground-based observations can be done at daily, monthly, seasonal and annual time scales in order to correct the biases (Rye et al., 2010). Several methods can be used to correct those errors, such as a simple bias shift toward observations (scaling or delta method) or either a matching of the two probability distributions (e.g. quantile mapping) (Rye et al., 2010). This step is important, as uncertainties in climate forcings are probably the main source of error in mass balance modelling (Østby et al., 2017).

The Canadian Rocky Mountains support many glaciers which provide water for hydropower production and agriculture and constitute iconic features highly valorized for tourism (Clarke et al., 2015; Comeau et al., 2009). Bolch et al. (2010) compared satellite images from 1985 to 2005 and reported an 11% (± 3.8%) loss of the glacier area in western Canada. A later study reported a 30% decrease in glacier surface area, representing 750 km^2 in the central and southern Canadian Rockies over the period 1919-2006, (Tennant et al., 2012). Only a few glaciers have been continuously monitored for mass balance in the Canadian Rockies. Peyto Glacier (51.67 °N, -116.53 °E) is the only reference site with a long mass balance record (1965-2019), which shows a consistent trend of negative annual balance beginning in the mid-1970's while the winter balance also appears to have decreased since then (Demuth and Pietroniro, 2003). No other long-term records exist to assess mass balance variations and trends in the region. Glacier models thus constitute important tools to estimate past and future mass balance variations for glaciers with scarce or no mass balance observations. A recent large-scale modelling study showed that the volume of western Canada's glaciers could decrease by 70% (± 10%) from 2005 to 2100, and will exceed 90% in the Rockies region (Clarke et al., 2015). Clarke et al. (2015) concluded that the main source of uncertainty in their simulations of glacier evolution at the mountain range scale was not the parameterisation of glacier flow but rather the simulation of surface mass balance. Thus, accurate models of surface mass balance are still needed at the scale of individual glaciers, in order to extend, and give context to, sparse mass balance observations as well as to characterize mass balance sensitivity to climate change. Saskatchewan glacier, the main outlet of the Columbia Icefield in the Canadian Rockies (52.15 °N, -117.29 °E), is such a glacier with

sparse mass balance observations available only since 2012. The objectives of this study are thus to reconstruct the mass balance of Saskatchewan Glacier using a physically-based model forced by reanalysis (NARR) data, to investigate spatio-temporal patterns of energy and mass balance fluxes, and to estimate the glacier mass balance sensitivity to a range of plausible future climate conditions.

Study area

The Columbia Icefield is a part of the Canadian Rocky Mountains and saddles the border of Alberta and British Columbia (in red on Fig. 1a). The Columbia Icefield is accessible via the Icefields Parkway which is surrounded by several national parks (Jasper, Yoho and Banff), which makes the Columbia Icefield a highly-valued cultural and touristic site (Clarke et al., 2015; Comeau et al., 2009). The plateau lying at an altitude of ~2800 m. above sea level (m a.s.l) intercepts moist air masses originating from the Pacific Ocean, which results in large snow accumulation and the formation of glacial ice flowing downward through several outlet glaciers. The interception of air masses in the main range of the Rocky Mountains creates a rain shadow effect in the front range, foothills and plains further east (Erler et al., 2015; Marshall et al., 2011). The Columbia Icefield is of crucial importance to the region's water budget, as it feeds three different continent-scale watersheds flowing towards the Arctic, Pacific and Atlantic seas (in blue Fig. **1**a). The main, and largest outlet glaciers are located to the east (Saskatchewan and Athabasca Glacier), draining around 60% of the eastern Columbia Icefields to the North Saskatchewan River (Atlantic) and the Sunwapta-Athabasca River (Arctic) (Marshall et al., 2011). Tennant and Menounos (2013) used historical aerial photographs and satellite images to reconstruct the extent and volume of the Columbia Icefield. Based on their study, they estimated that the area of the Columbia Icefield was 265.1 ± 12.3 km^2 in 1919 but that it had declined by 59.6 ± 1.2 km^2 in 2009 at a rate of -0.66 ± 0.01 $km^2\ a^{-1}$. Saskatchewan Glacier experienced the greatest absolute area loss at 10.1 ± 0.6 $km^2\ a^{-1}$. Saskatchewan Glacier is the largest outlet glacier of the icefield, covering an area of roughly 23 km^2 and ranging in elevation from 1784 to 3322 m (Ednie et al., 2017). It was discovered by early explorer Walter Wilcox from Parker Ridge in 1896 and began to be

mapped and photographed between 1924 and 1949 by pioneer glaciologist William O. Field (Heusser, 1956). Ice flow was first studied on Saskatchewan Glacier in 1952-54 using theodolites (Meier, 1960), then studied in 1998 with the use of airborne RADAR (Mattar et al., 1998). Daily movement of 35 cm per day in the central part of the glacier and a maximum ablation rate of 7.5 cm d^{-1} were measured (Meier, 1960; Mattar et al., 1998). The Geological Survey of Canada (GSC) initiated a mass balance measurement program on Saskatchewan Glacier in 2012. The Columbia icefield is located 70 km northwest of Peyto Glacier, which is situated in a drier, continental climate (Demuth and Pietroniro, 1999). Beginning in 1966, Peyto Glacier has the longest mass balance observation record in Canada and is thus an important reference site to assess glacier health in the central Canadian Rockies (Demuth et al., 2006), which makes it interesting to compare with the reconstructed mass balance on Saskatchewan Glacier.

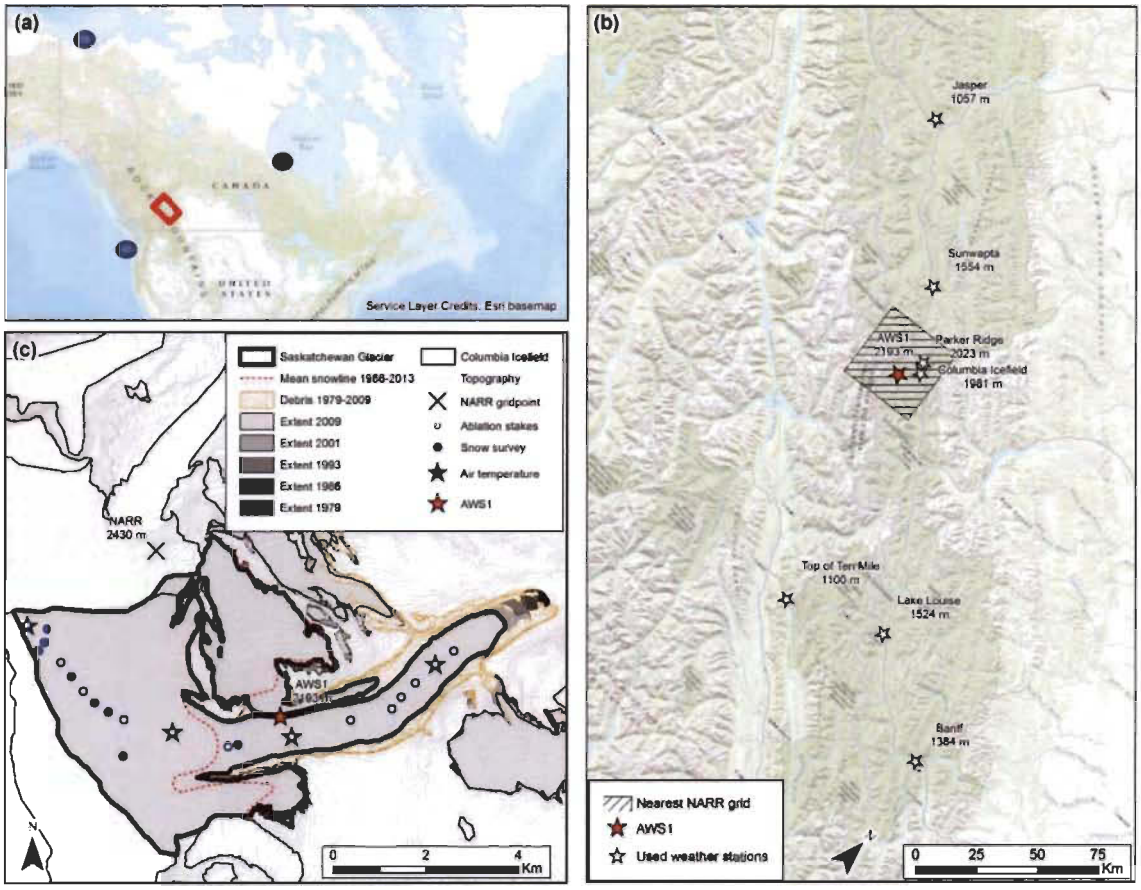

Fig. 1 Study area map. (a) Location of the Columbia Icefield in the Canadian Rockies. (b) Stations from the permanent network chosen to calculate temperature and precipitation lapse rate. The nearest NARR gridpoint (hatched square) is located directly above Athabasca Glacier and encompasses Saskatchewan Glacier. (c) Map of Saskatchewan Glacier showing the location of ablation stakes and additional snow survey points, and air temperature sensors used to determine the mean diurnal lapse rate over the glacier. The mean snow line position (1986-2013) is shown by a red dotted line.

Data and Methods

Glaciological observations

Topographic data

The main topographic data used in this study is a 1-meter resolution digital elevation model (DEM) derived from two WorldView-2 (WV2) satellite stereo images acquired on July 31, 2010, covering the lower glacier and September 18, 2010, covering the upper glacier. The merged DEM covers the whole glacier and surrounding topography. It was further extended with tiles from the Canadian Digital Surface Model (CDSM) (20-meter resolution) in order to include all topography susceptible to cast shadow on the glacier. The merged DEM was resampled to 100 meters resolution using nearest neighbour interpolation to allow faster calculation with the mass balance model. The resulting grid is comprised of 355 columns and 300 rows, and has approximately the same extent as the NARR gridpoint used for model forcing (Fig. 1b). The glacier extent of August 2009 from Tennant and Menounos (2013) was used as boundary of the 2010 WV2 DEM. The slope, aspect and sky-view factors were derived from this DEM with ArcGIS toolboxes in order to be used as inputs in the mass balance model. The firn area was delimited by a mean snowline delineated from LANDSAT satellite images from year 1986 to 2013 (Fig. 1c). 18 cloud-free images were chosen near the end of the hydrological season (September 30) and used to map the mean snowline position at the end of summer. Image dates ranged between August 22 and October 2, which was necessary to find cloud-free images close to the end of the ablation period to provide the best estimate of the equilibrium line altitude (ELA) as possible (Fig. 1c). To take into account historical glacier recession in mass balance simulations, multi-temporal DEMs and glacier boundaries from Tennant and Menounos (2013) were used to update the glacier geometry over time in the mass balance model. Only the area inside the glacier extent were updated from the main DEM for every year available (1979; 1986; 1993; 2001) except 2009. We used spline spatial interpolation to convert the elevation point of Tennant and Menounos (2013) into a grid. We used the glacier extents to extract and merge the interpolated elevations on the glacier with the off-glacier topography of the main DEM (2010). We discarded the elevation points of Tennant

and Menounos (2013) for 2009 because the points in the accumulation area were not dense enough to perform the spatial interpolation. The WV2 2010 DEM was used instead in the dynamical mass balance simulation. Two static mass balance simulations were performed using the 1979 and 2009 geometries and compared with the dynamical simulation in which the glacier geometry was adjusted when DEMs were available (1979; 1986; 1993; 2001; 2009), in order to see the impact of glacier recession on mass balance. The sensitivity analysis was performed using the GLIMS extent of 2011 before we had access to elevation points and glacier extents of Tennant and Menounos (2013). An ArcGIS model builder with every manipulation and parametrization of the DEMs is available in the supplementary material.

Mass balance observations

Mass balance is measured by the GSC since 2012 using the glaciological method (Ednie et al., 2017) and the observations available were used to validate the modelled mass balance. End-of-winter mass balance observations (bw) include snow depth soundings at, and between ablation stakes along the glacier centerline (Fig. **1**c). Snow depth were converted to snow water equivalent (SWE) using snow density measured at a network of reference snowpits dug in the accumulation zone, near the ELA and in the ablation zone, and complemented by snow cores (Ednie et al., 2017). End-of-summer ablation (bs) was measured at a network of 13 stakes along the glacier centerline (Fig. 1c). The number of bs observations varied between years due to some stakes emerging completely from the ice surface and falling off before field visits, or because stakes in the upper part of the glacier could sometimes not be reached by foot during field visits. bw observations are more numerous because the upper glacier was accessed by helicopter at the end of winter and the surveys done on skis, and because additional snow soundings were made between ablation stakes. The annual mass balance (ba) was calculated by summing the winter and summer balance data. The data obtained over these 5 years were used to validate the mass balance of the model.

A second, independent validation was performed by comparing the mass balance reconstructed by the model with cumulative geodetic mass changes from 1979 to 2009 estimated by Tennant and Menounos (2013). Tennant and Menounos (2013) created multi-temporal DEMs of the entire Columbia Icefield using Interprovincial Boundary Commission Survey (IBCS) maps for glacier extent and photogrammetry of aerial photographs from 1979, 1986 and 1993. For year 1999, they used a 30 m resolution Landsat 5 Thematic Mapper (TM) Image of September 2001 for glacier extent and the Shuttle Radar Topography Mission (SRTM) DEM of February 2000, which they attributed to best represent the glacier surface at the end of the 1999 summer ablation season, due to the penetration of the radar wave in the following year's winter snowpack. Finally, they used a Satellite Pour l'Observation de la Terre 5 (SPOT 5) images with a resolution of 2.5 m for the year 2009. Points matched on stereoscopic image pairs were gridded to a 100 m resolution in the ablation area and to 200 m in the accumulation area where low contrasts resulted in a smaller number of elevation points. The point clouds were interpolated to a continuous DEM surface with a resolution of 100 m to allow their comparison with the simulated mass balance. The uncertainties on elevation changes were determined by analyzing elevation changes on stable terrain around the icefield (Tennant and Menounos, 2013).

Meteorological data

On-glacier automatic weather stations

An automatic weather station (AWS) was deployed in August 2014 on the medial moraine of Saskatchewan Glacier at an altitude of 2193 m a.s.l. and operated hourly for a 2-year period, until August 2016 (Fig. 1c). Recorded variables include air temperature (Ta), relative humidity (RH), incoming (SWin) and reflected (SWout) solar radiation, and wind speed (WS) and direction (WD). The station fell down on June 2015 due to a crevasse opening next to the station, which caused a one-month data gap. The station was fortunately and kindly rescued by a mountaineer visiting the glacier, who secured the station back up. The movement of the moraine caused the station to fall again during the following summer, terminating the data collection in June 2016. *HOBO* air temperature

sensors were installed by the GSC on five ablation stakes (Fig. 1c) between May to August 2015, shielded from solar radiation using naturally ventilated shields. The data were used to calculate a mean diurnal cycle for the air temperature lapse rate on the glacier, as diurnal variations in the lapse rate have been shown to affect glacier melt simulations: Petersen and Pellicciotti (2011) found that prescribing a diurnal lapse rate was important because melting occurs mostly during the day when the lapse rate was steeper than at night. The mean diurnal cycle for the glacier lapse rate was combined with a monthly lapse rate estimated from the permanent weather station network (see next section).

Meteorological data from permanent weather monitoring network

Mean monthly air temperature lapse rates and a constant precipitation lapse rate were calculated from the permanent weather monitoring network maintained by Environment and Climate Change Canada. Seven weather stations with available air temperature data during the study period were chosen, ranging in elevation from 1050 to 2025 m a.s.l. (Fig. 1b). A mean monthly lapse rate was calculated by linear regression of mean temperature against elevation, using a minimum of five stations for each month depending on available data. Diurnal anomalies in the glacier lapse rate calculated in the previous section were added to the monthly lapse rates. As precipitation was not measured at the AWS site, an homogenized historical precipitation record was produced using data from the two weather stations closest to Saskatchewan glacier (Parker Ridge, 2023 m a.s.l. and Columbia Icefield, 1981 m a.s.l., see Fig. 1b), and used to downscale the NARR precipitation data. The Columbia Icefield station was only operated between May and November while Parker Ridge was operated mostly in winter and sometime all year-round depending on road accessibility. Both records were combined into a single homogenised record, but data gaps remained and the disparate nature of the precipitation record explains why the continuous NARR precipitation data was used instead of the observations. As the glacier mass balance model only considers a constant precipitation lapse rate, a single lapse rate was calculated from the weather station network for the months of October to April, when snow precipitations are most abundant on the glacier.

Reanalysis data

While the precision of the on-glacier AWS data is useful to characterize the glacier microclimate, its short and discontinuous record is not adequate to drive a physically based, distributed glacier mass balance model over a longer historical period. Therefore, meteorological reanalysis data were used to force the mass balance model over the 1979-2016 period, and the AWS data used to apply a first-order bias correction to the reanalysis data. Data from the NARR were chosen for this study because of its higher temporal (3 h) and spatial (32 km) resolution compared to other commonly used products, such as ERA interim and NCEP reanalyses. NARR data for the gridpoint closest to Saskatchewan glacier (see Fig. 1) were acquired from the National Center for Environmental Prediction (NCEP) at the National Centers for Atmospheric Research (NCAR). The NARR gridpoint elevation is 2430 m a.s.l., i.e. 237 m higher than the elevation of the glacier AWS used to downscale the data. The following variables were used: instantaneous values of air temperature and relative humidity values at 2 m above the surface (TMP2m-ANL, RH2m-ANL), wind speed vectors at 10 m above the model surface (U and V wind components: UGRD10m-ANL, VGRD10m-ANL), surface 3-hourly accumulated precipitation (APCPsfc-ACC), 3-hourly averaged surface downward shortwave radiation fluxes (DSWRFsfc-AVE) and instantaneous values of total cloud cover (CC: TCDCclm-3hr). The 3-hourly data were interpolated to an hourly interval using linear interpolation and compared with the glacier AWS observations from 2014-2016. 3-hourly NARR variables were interpolated to the center of the hourly averaging interval used by the AWS datalogger, but attributed an end-of-the hour time tag as used by the datalogger. For instantaneous variables (ANL) the concurrent time tag was used for the interpolation while for averages (AVE) the time at the center of the averaging interval was used. The 3-hourly accumulated (ACC) precipitation totals were disaggregated to hourly values by dividing the 3-hour totals into three exact quantities. Both the incoming solar radiation and air temperature have strong diurnal cycles. Over the year, solar noon varies between 12 h 41 to 12 h 56 and sunshine duration between 7 h 45 to 16 h 45. The 3-hourly NARR data could thus underestimate the daily peaks in solar radiation and air temperature, especially since midday NARR 3 hourly average value spreads between 11 h 00 and 14 h 00. However, given that solar noon occurs near the

middle of this interval the NARR midday solar radiation average may in fact well approximate the peak mid-day value, while the 14 h 00 instantaneous temperature value is close to the time of maximum daily temperature. Still, to reduce the probability of the diurnal cycle being attenuated in the interpolated NARR data, a shape-preserving piecewise cubic interpolation was used to interpolate these variables to an hourly interval.

The NARR meteorological variables were downscaled to the AWS site using a simple bias correction procedure (Cannon et al., 2015; Wetterhall et al., 2012) using Meteo Lab (ML) Matlab® Toolbox. As precipitation was not measured at the glacier AWS, the homogenized historical precipitation record was used to downscale the NARR precipitation data. Three simple bias correction methods were tested (scaling, delta and empirical quantile mapping - EQM) and applied to the temperature, relative humidity, wind speed and precipitation data. Because errors in incoming solar radiation can originate from improper representation of the atmospheric transmissivity and cloud cover in NARR, but also from differences in shading between the NARR smoothed topography and the real topography, a time-varying scaling bias correction method was used to correct the NARR shortwave radiation data. A mean diurnal multiplicative correction factor was calculated by scaling the mean observed diurnal SWin cycle with that of the hourly-interpolated NARR. A separate diurnal correction factor was calculated for each month of the year, to account for the seasonality in sun angle and related errors between NARR and observations. The bias correction methods were evaluated against the glacier AWS data using split sample cross-validation, and compared with the baseline performance, i.e. without corrections to the NARR variables. The AWS data was split into two one-year sub-periods; downscaling methods were calibrated on one period and validated on the other, and then both sub-periods were inverted, and the mean validation statistics calculated. For precipitation the whole historical record was used, so validation sub-periods are longer than for other variables. The Pearson correlation coefficient (R), mean error (bias), root mean square error (RMSE) and mean absolute error (MAE) were used for performance assessment. The downscale performance was evaluated at both hourly and daily time intervals.

Mass balance model

The physically based, distributed glacier mass balance model DEBAM (Hock and Holmgren, 2005) was used to simulate the mass balance of Saskatchewan Glacier over the period 1979-2016. The surface mass balance can be expressed as:

$$b(t) = Ps(t) - M(t) - S(t) \quad (1)$$

Where $b(t)$ is mass balance at time t, Ps is snow precipitation, M is melt and S is sublimation. Total precipitation is extrapolated to the model grid from the altitude of the homogenized reference station (2000 m a.s.l.) using a constant gradient calibrated from weather stations (cf. section 2.Albedo). Total precipitation is split between rain and snowfall according to a threshold temperature ($T0$) of 1.5 °C referring to a median RH of 83% at the AWS (DeWalle and Rango, 2008). The ideal threshold for humidity between 80 and 90% is 1.4 °C (Jennings et al., 2018). Continental areas and mountain ranges generally exhibit the warmest thresholds, which support the value of 1.5 °C used in the model. When the air temperature is at $T0$, 50% of the precipitation falls as snow and 50% as rain. A linear interpolation of the rain/snow fraction is performed between $T0$-1 °C (100% snow) and $T0$+1 °C (100% rain). As snowfall notoriously suffers from undercatch in mountainous regions (Fassnacht, 2004; Rasmussen et al., 2012), a precipitation correction factor (PCF, in %) was applied to the precipitation data after calibrating the modelled snow cover against snow survey observations.

The model calculates the distributed mass and energy balance on each gridcell from hourly meteorological forcing data including air temperature, relative humidity, precipitation, wind speed and incoming shortwave radiation (SWin). The energy at the surface available for melt on the glacier, Q_M (W m^{-2}), was calculated according to Eq. (2) and converted into meltwater equivalent M (mm h^{-1}) using the latent heat of fusion:

$$Q_M + Q_G + Q_R + Q_L + Q_H + L\uparrow + L_S\downarrow + L_T\downarrow + (1-\alpha)(I + D_S + D_T) = 0 \quad (2)$$

where I is the direct (beam) incoming shortwave solar radiation, D_S and D_T are the diffuse sky and terrain shortwave radiation, respectively, α is the albedo, $L_S\downarrow$ and $L_T\downarrow$

are the longwave sky and terrain irradiance, respectively, L ↑ is longwave outgoing radiation, Q_H is the sensible-heat flux, Q_E is the latent-heat flux, Q_G is the ground heat flux in the ice or snow and Q_R is the energy supplied by rain (Hock and Holmgren, 2005). All fluxes are positive toward the glacier surface and measured or calculated in W m^{-2}. The model allows for different parameterizations for calculating energy balance components, depending on the availability of forcing data and calculation speed. The parameterizations used in this work are detailed in the next subsections.

Shortwave incoming radiation

In this study, the incoming shortwave radiation (SWin) from downscaled NARR at the AWS location is separated into the direct (I) and diffuse (D) components, which are then extrapolated individually to each gridcell considering terrain effect of the multi-temporal DEMs. The separation is based on an empirical relationships between the ratio D/SWin and the ratio of measured SW_{IN} to the top-of-atmosphere radiation, SWin/I_{TOA}, following Hock and Holmgren (2005). Total diffuse radiation D calculated at the AWS is then subtracted from the global radiation to yield the direct solar radiation at the AWS site, I_S. Topographic shading is calculated at each hour and for each gridcell from the path of the sun and the effective horizon. If the AWS is shaded by surrounding topography, any measured global radiation is assumed diffuse. Direct radiation I is obtained at each gridcell from:

$$I = \frac{I_S}{I_{SC}} I_C \tag{3}$$

where the subscript s refers to the location of the climate station and c denotes clear-sky conditions. I_C is the potential clear-sky direct solar radiation which account for the effects of slope and aspect of each gridcell on radiation, as well as shading from surrounding topography. The ratio I_S/I_{SC} measured at the AWS accounts for deviations from clear-sky conditions, expressing the reduction of potential clear-sky direct solar radiation mainly due to clouds, and is assumed to be spatially constant. Eq. (3) can not be applied when the AWS is shaded, since $I_C = 0$. In this case and for glacier gridcells still illuminated the last ratio that could be obtained before the AWS gridcell became shaded

is applied, which assumes that cloud conditions remain constant until the climate station is illuminated again, usually the next morning. The impact of this assumption on the radiative balance is assumed to be small because this situation occurs at low sun illumination angles.

The total diffuse radiation (D) is calculated as:

$$D = D_0 F + \alpha_m SWin(1 - F) \quad (4)$$

Where the first righthand term in Eq. 2 represents sky radiation (D_S) and the second term terrain radiation (D_T). D_0 is diffuse radiation from an unobstructed sky calculated at the AWS and is considered spatially constant. F is the gridcell sky-view factor defined by Oke (1987) and SWin is the downscaled NAAR global radiation at the AWS. α_m is the mean albedo of the surrounding terrain obtained for every hour as the arithmetic mean of the modelled albedo of all gridcells of the entire glacier (Hock and Holmgren, 2005).

Albedo

The albedo parameterisation of Oerlemans and Knap (1998) was used to simulate the albedo (α):

$$\alpha_{snow}(t) = \alpha_{firn} + (\alpha_{frsnow} - \alpha_{firn}) exp\left(\frac{s-t}{t^*}\right) \quad (5)$$

$$\alpha(t) = \alpha_{snow}(t) + \alpha_{ice} - \alpha_{snow}(t)\, exp\left(\frac{d}{d^*}\right) \quad (6)$$

where $\alpha_{snow}(t)$ is snow albedo and $\alpha(t)$ the final glacier albedo at time t, α_{firn} is the characteristic albedo of firn, α_{frsnow} is the characteristic albedo of fresh snow and α_{ice} is the characteristic albedo of ice. t^* is the time scale determining how fast the snow albedo decays over time and approaches the firn albedo after a fresh snowfall and d^* is a characteristic scale for snow depth controlling the transition from snow albedo to ice albedo. S is the day of the last snowfall and d is snow depth. The constant, characteristic albedo values were set to α_{frsnow} = 0.9 for fresh snow based on observations at the AWS,

and to α_{ice}= 0.3 for ice based on direct and remote-sensing estimates on neighbouring Athabasca glacier (Gratton et al., 1993; Bordeleau, 1998) and Peyto Glacier (Nakawo and Young, 1981) which presents similar facies in the ablation zone. Firn albedo was set to α_{firn}= 0.6 (Cuffey and Paterson, 2010 p. 146). The characteristic time (t^*) and depth (d^*) scales were calibrated using snow depth and albedo measurements at the AWS. Since the AWS was on a moraine the value for α_{ice} was set instead to the measured soil albedo for calibration purpose. The optimum values found, t^* = 14 day and d^* = 3 cm, where used in the model.

Atmospheric incoming longwave calculation

The calculation of atmospheric incoming longwave radiation (LWin) is based on Konzelmann et al. (1994) which relies on independent variables of air temperature, vapour pressure and cloud cover:

$$LWin = [\varepsilon_{cs}(1 - n^p) + \varepsilon_{oc} n^p]\sigma Ta^4 \quad (7a)$$

$$\varepsilon_{cs} = 0.23 + 0.443\left(\frac{e}{Ta}\right)^{1/8} \quad (7b)$$

where ε_{cs} is the clear-sky emissivity, n is the fractional cloud cover fraction (0-1) derived from NARR CC data (in okta), σ is the Stefan-Boltzmann constant (5.67×10^8 m^{-2} K^{-4}) and Ta is the downscaled NARR air temperature in Kelvin. The overcast sky emissivity (ε_{oc} = 0.968) and exponent p = 2, were left to default values in DEBAM. We adjusted the emissivity calculation in DEBAM to include the spatial variability in air temperature since the default parameterisation only used Ta measured at the AWS location for the entire glacier area. This led to an overestimation of melt in the accumulation zone and an underestimation in the ablation zone, which was corrected when including the distributed Ta in Eq. 7a.

Turbulent heat fluxes

The turbulent sensible (Q_H) and latent (Q_E) heat fluxes were calculated from the bulk aerodynamic method (Hock and Holmgren, 2005) based on air temperature (Ta), wind speed (WS) and vapour pressure (e_z) at height (z) above the surface:

$$Q_H = \rho C_p \frac{k^2}{\left[ln\left(\frac{z}{z_{0w}}\right)-\psi_M\left(\frac{z}{L}\right)\right]\left[ln\left(\frac{z}{z_{0T}}\right)-\psi_M\left(\frac{z}{L}\right)\right]} WS_z(Ta_z - T_0) \quad (8)$$

$$Q_E = L_v \frac{0.623\rho_0}{P_0} \frac{k^2}{\left[ln\left(\frac{z}{z_{0w}}\right)-\psi_M\left(\frac{z}{L}\right)\right]\left[ln\left(\frac{z}{z_{0e}}\right)-\psi_M\left(\frac{z}{L}\right)\right]} WS_z(e_z - e_0) \quad (9)$$

where ρ is the air density at sea level (1.29 kg m^{-3}), P_0 is the mean atmospheric pressure at sea level (101325 Pa), C_p is the specific heat capacity of air (1005 J kg^{-1} K^{-1}), k is the von Kármán's constant (0.4), T_0 is the surface temperature, e_0 is the surface vapour pressure, z_{0w}(1.3 mm), z_{0T} and z_{0e} are the roughness lengths for the logarithmic profiles of wind speed, temperature and water vapour, respectively, ψ_M, ψ_H and ψ_E are the stability functions, L is the Monin–Obukhov length, and L_v is the latent heat of evaporation (2.514 × 10^6 J kg^{-1}) or sublimation (2.849 × 10^6 J kg^{-1}), depending on surface temperature and the direction of the latent heat flux. If Q_E is positive and the surface is melting the surface experiences condensation, else deposition if the surface is frozen. Sublimation occurs when Q_E is negative. The aerodynamic roughness length for snow and ice influences the intensity of turbulent fluxes at the glacier surface. Typical z0 values for melting ice in ablation zones range between 1 and 10 mm (Brock et al., 2006; Munro, 1989), while smooth ice value can range between 0.1 and 3 mm (Brock et al., 2006), e.g. a mean of 2.4 mm (Brock et al., 2006) and 2.7 mm (Hock and Holmgren, 1996). As this parameter was not measured it was calibrated within a 1-10 mm range against annual mass balance observations (ba). z0 for snow was calibrated on ba between 1.3 and 3.25 mm. The roughness length for temperature and water vapour were both considered to be two orders of magnitude less than roughness lengths for wind.

Model validation

The simulated mass balance was validated at the point-scale against available seasonal and annual glaciological mass balance observations since 2012, and at the glacier scale using the reconstructed geodetic mass balance from 1979 to 2009 from Tennant and Menounos (2013).

Climate sensitivity

Air temperature is a key factor on glacier annual mass balance because of its influence on the precipitation phase and melting rates (Cuffey and Paterson, 2010, p. 104). We used the calibrated and validated DEBAM model to perform a static (e.g. with fixed 2010 glacier geometry, see Oerlemans (2001)) climate sensitivity analysis of mass balance to potential changes in air temperature (ΔTa) ranging between 0 to 8 °C and precipitation (ΔP) ranging between -20 to +20%. In total DEBAM was run 81 times for every combinaison of ΔTa and ΔP perturbation imposed on Ta and P records over a 20-year reference period (1981-2000). This reference period was chosen since the time interval (20 years) matches that used in climate projections scenario (2046-2065 and 2081-2100). Changes in mass balance for each sensitivity run were plotted as response surfaces, which provide a simple way to assess climate sensitivity across a range of possible climate change scenarios e.g. Prudhomme et al. (2010). Ensemble GCM simuations from the CMIP5 project (IPCC AR5 Atlas subset) were obtained from KNMI Climate Change Atlas (Van den Hurk et al., 2007; Trouet and Van Oldenborgh, 2013) for the gridpoint 52.134258 °N, -117.228629 °E. Ensemble simulations were used for RCP scenarios +2.6 (n = 32), +4.5 (n = 42), +6.0 (n = 25) and +8.5 (n = 39) for the mid (2046-2065) and late (2081-2100) 21st century (IPCC, 2012). Mean temperature and precipitation changes along with their 90% confidence intervals were overlained onto the response surfaces to show the most likely future climate trajectories given by the latest projections from climate models.

Results

Model forcing and calibration

Meteorological data

Daily and monthly averages of air temperature (Ta), relative humidity (RH), incoming solar radiation (SWin) and wind speed (WS) measured at the glacier AWS between August 2014 and August 2016 are plotted in (Fig. 2). The period with missing data at the end of June 2015 corresponds to the station falling down following the opening of a crevasse on the medial moraine. The winter of 2014-2015 was overall colder than 2015-2016, with frequent cold excursions below -15 °C and a winter absolute minimum of -27 °C vs. -17 °C in 2015-16, although conditions were warmer in December. Relative humidity is generally high throughout the year (mean = 79%), illustrating the predominantly humid climate of the Columbia Icefield, but decreases noticeably in summer. The variability in daily RH is similar between the two years of measurements. The monthly incoming solar radiation (SWin) shows a pronounced seasonal cycle, varying roughly between 50 W m^{-2} in winter and 300 W m^{-2} in summer, with daily variations between 50 W m^{-2} in winter and 150 W m^{-2} in summer caused by variable cloud cover. The wind speed is generally high (mean = 16 m s^{-1}) but shows significant day-to-day variations, and with generally higher wind speed recorded in winter and lower values in summer. A gradual increase in wind speed is notably observed from the lowest monthly mean value in May 2015 (6 m s^{-1}) to a maximum in February (26 m s^{-1}). The homogenized historical precipitation record from the Columbia Icefield and Parker Ridge stations contains several gaps but still portray the seasonal and interannual variability in precipitation near the glacier (Fig. 3). The monthly mean precipitation throughout the historical period is 73 mm $month^{-1}$ (874 mm a^{-1}) but varies annually between 23 mm mo^{-1} and 142 mm mo^{-1}. The winter is the season with the most precipitation (58% of precipitation fell between October to March, mostly as snow) while the cumulative precipitation in summer is lower (42% of precipitation mostly as rain).

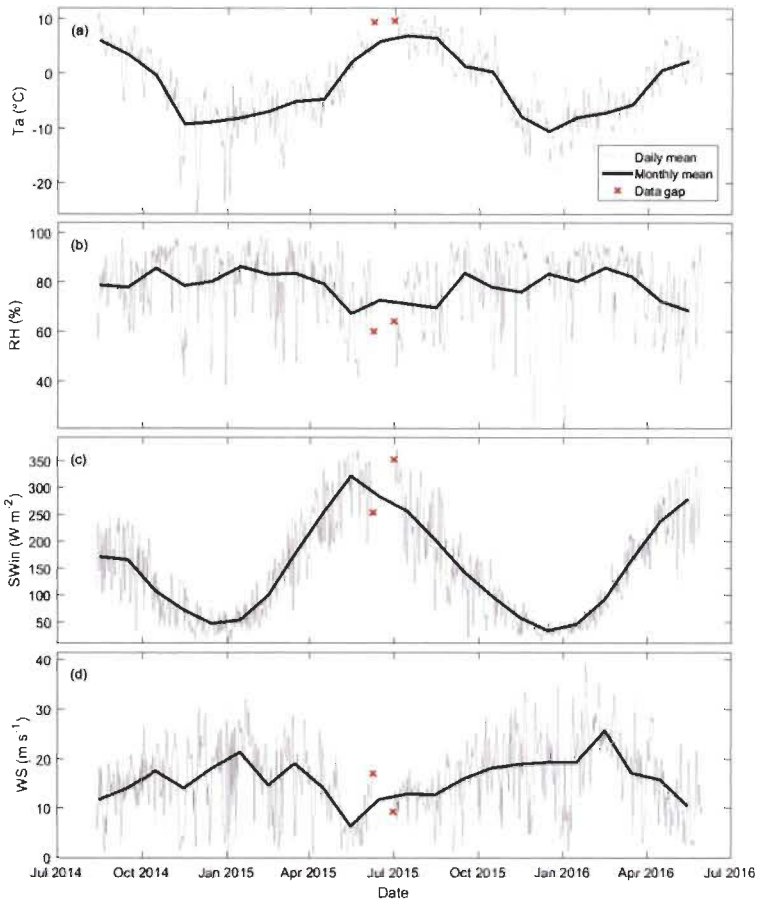

Fig. 2 Two-year record from the AWS operated on Saskatchewan Glacier (2014-2016). (a) Air temperature (Ta); (b) relative humidity (RH); (c) incoming solar radiation (SWin); (d) wind speed (WS). The red cross indicates the date on which the AWS fell into a crevasse and was replaced after less than a month (11 to 30 June 2015).

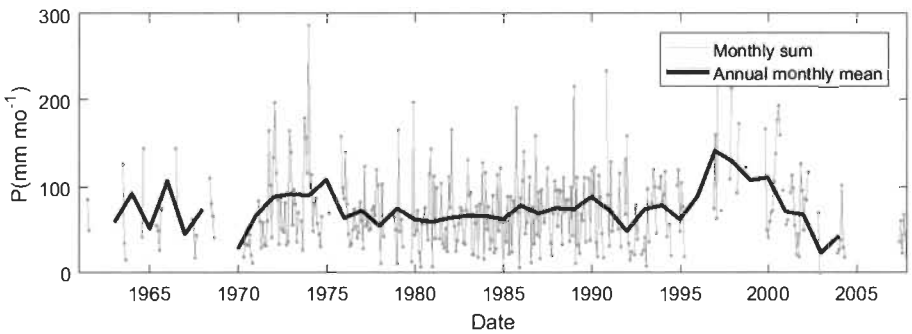

Fig. 3 Homogenized historical precipitation record. Solid grey line: monthly sum precipitation (total of 34 months between 11-28 days and 300 months are higher than 28 days); solid black line: annual sum recorded.

NARR bias correction

The NARR meteorological variables used to drive the glacier model were compared with data from the glacier AWS (2014-16) and the 29-year long nearby homogenized daily precipitation record (Table 1). Results show that even without applying bias correction Ta, RH and SWin show a good correlation on daily value with the NARR data, which indicates that the diurnal and seasonal variability of these variables is well represented in the NARR product. The correlation is poorer for WS, likely because the local glacier katabatic wind recorded by the AWS is not well represented in NARR due to its coarse grid resolution. The NARR precipitation is also rather poorly correlated with observations. Precipitation are notoriously more difficult to represent in reanalysis products, especially in mountainous terrain with steep orographic gradients and localized convective activity (Hofer et al., 2010; Mesinger et al., 2006). The accuracy measure (Bias: NARR 2430 m a.s.l. minus AWS 2193 m a.s.l.) is negative for Ta, WS and RH but relatively small compared to the mean and range of values recorded (Fig. 2), except for SWin (30.41 W m^{-2}) and P (0.55 mm d^{-1}), which are positive and represent 15% and 25% of their mean measured values over their period of observation, respectively.

All correction methods did not improve the Pearson correlation coefficient (R), as R is a relative measure of the synchronicity between two-time series and is unaffected by the mean values. The EQM method was found to improve Ta best, closely followed by the scaling method. Validation statistics were most improved using the scaling technique for precipitation and WS, while the diurnal scaling correction applied to SWin also reduced its errors. None of the method were found to improve the errors in relative humidity, which had an initial low error. The scaling method was globally the more efficient approach across all variables and this method was thus applied to all variables for consistency, except for relative humidity which was left uncorrected. Similar results, although with expectedly higher errors, were found for the interpolated NARR hourly data (Supplementary Table 1). Bias corrections were thus calibrated on daily values only.

Table 1. Statistical downscaling of NARR data using a two-year AWS record and the 29-year homogenized historical precipitation record. The daily validation is first done over the entire period before bias correction ('no downscale'). Validation statistics for each bias correction methods are the mean of the two left-out daily validation periods (see methods). R = Pearson correlation coefficient; RMSE = root mean square error; Bias = mean error (NARR minus AWS); MAE = mean absolute error. Values in bold indicate the best value across all methods.

Method	Statistic	Ta (°C)	WS ($m\ s^{-1}$)	RH (%)	SWin ($W\ m^{-2}$)	P ($mm\ d^{-1}$)
No downscale	R	**0.98**	**0.37**	0.85	0.92	**0.30**
	RMSE	1.94	2.30	**7.96**	52.72	5.22
	Bias	-1.26	-1.12	-0.09	30.41	0.55
	MAE	1.57	1.85	6.17	38.51	3.10
Scaling	R	0.98	0.37	0.85	**0.93**	0.30
	RMSE	1.49	**2.21**	7.97	**39.08**	**4.96**
	Bias	**0.00**	**0.00**	0.03	**-0.25**	**0.00**
	MAE	1.16	**1.72**	6.15	**29.10**	**2.82**
Delta	R	0.97	0.37	0.85	-	0.26
	RMSE	1.88	2.33	8.40	-	6.01
	Bias	**0.00**	**0.00**	**0.02**	-	0.01
	MAE	1.34	1.82	6.34	-	3.09
EQM	R	0.98	0.37	**0.86**	-	0.26
	RMSE	**1.39**	2.33	8.06	-	5.92
	Bias	0.03	-0.01	-0.11	-	-0.03
	MAE	**1.04**	1.82	**6.04**	-	3.06

Monthly and annual averages of the bias-corrected NARR variables used to drive the model are displayed in Fig. 4. There is no visible trend in mean annual Ta over the 30 years period, but there is a noticeable increase in minimum temperatures, with e.g. only two years with a monthly mean colder than -15 °C in 2000-2015 compared to seven years between 1980-1995. The positive trend seen in annual mean RH is driven by increasing annual minima while annual maximum show no trend, such that the seasonal amplitude decreases over time. A monthly average of RH over the entire period reveals that the months of July and August have lower values (mean = 72%) while the winter months are higher (mean = 80-82%) (Fig. 2b). No clear trends occur in annual cloud cover (CC) and SWin, despite the trend in RH. The largest annual deviations in CC, e.g. after 2005, are reflected by inverse fluctuations in SWin, reflecting the attenuation of solar radiation

by clouds. A progressive decline in WS occurs from 1979, reaching the lowest annual value of the period in 1995 (~4.3 m s^{-1}). A more subdued increase in WS occurs afterward until 2010, followed by a decline. Finally, mean monthly precipitation shows no long-term trend but significant seasonal and interannual variability. The seasonal amplitude decreases after 2000, mostly driven by increasing seasonal minima decrease of monthly mean over 150 mm mo^{-1}. The annual trend is still variable, but we can see a little increase in the annual amount of precipitation for the last year in comparison with the global mean.

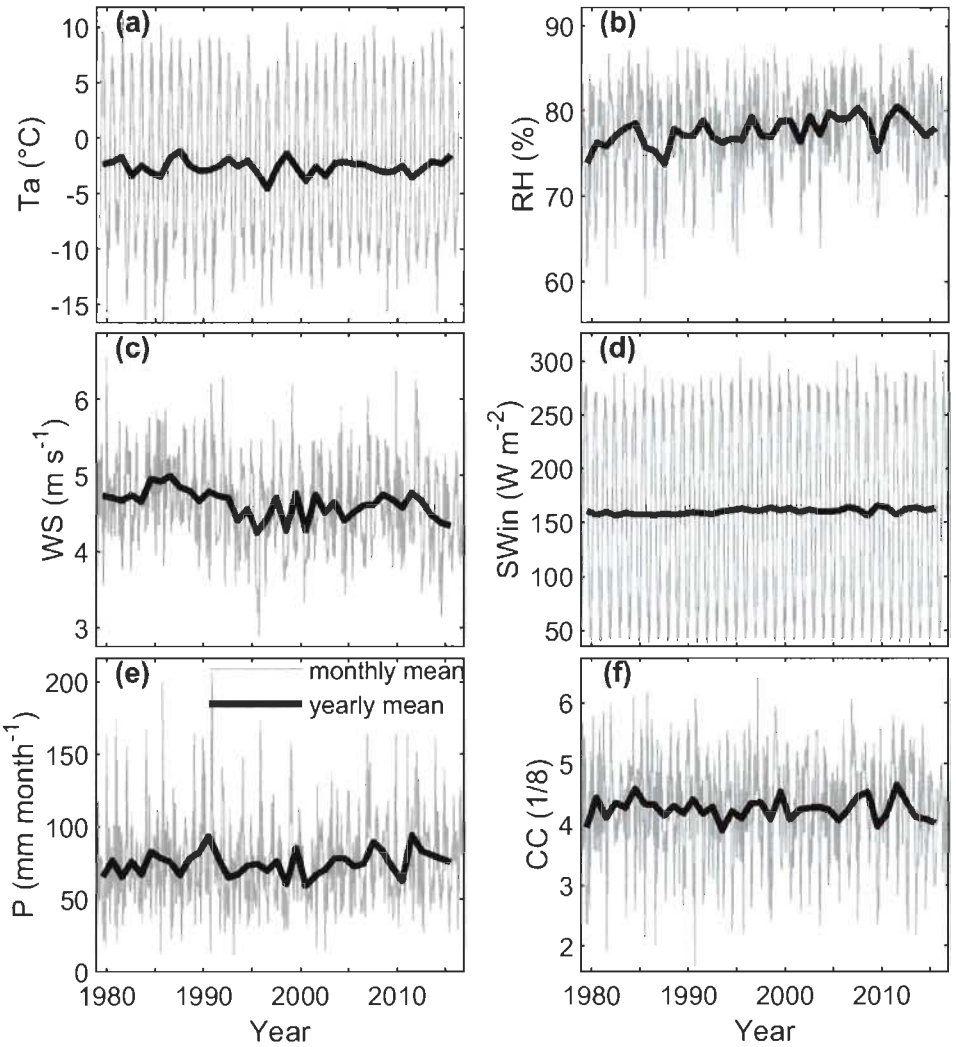

Fig. 4 Downscaled NARR variables used to drive the DEBAM model. Grey solid lines represent monthly means and black solid lines represent annual averages.

Lapse rate

On-glacier diurnal air temperature lapse rates were found to vary between -0.55 °C $100m^{-1}$ at night and to increase during the day, reaching a maximum of -0.34 °C $100m^{-1}$ at midday (Fig. 5a). The strength of the temperature-elevation relationship, as measured by the correlation coefficient (R), is generally high ($R > 0.95$) but decreases slightly during daytime hours ($R = 0.92$). In fact, the lapse rates was quite constant at night due to the absence of the sun effects on surface temperature, while differential heating between the glacier tongue and upper accumulation area during the day and associated local wind regimes (katabatic vs. valley wind) could explain the partial breakdown of the relationship and the smaller lapse rates. On a monthly scale the lapse rate varied between -0.58 °C 100 m^{-1} and -0.42 °C 100 m^{-1} without any systematic seasonal pattern. The correlation of the annual lapse rates is also more variable then diurnal lapse rates, varying between low values ($R = 0.6$) in winter to higher values ($R = 0.94$) in summer. Diurnal lapse rate anomalies, calculated as deviation from the mean diurnal lapse rate (Fig. 5a), where added to the monthly lapse rates (Fig. 5b) and used to distribute air temperature to the glacier surface.

Seven weather station were used to calculate a constant precipitation lapse rate. Since most snow precipitation falls on Saskatchewan Glacier during October-April when temperatures are below freezing, a mean lapse rate of 14.2% 100 m^{-1} calculated during October-April was initially used in the model to extrapolate precipitation from the reference station.

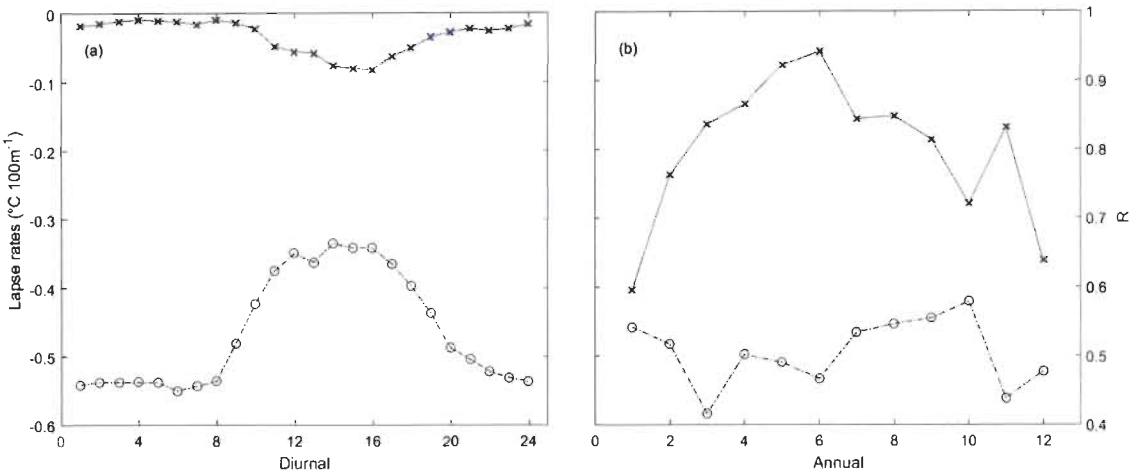

Fig. 5 Calculated air temperature lapse rates. The black axis represents the air temperature lapse rate in °C 100 m^{-1} while the blue axis represents the correlation coefficient (R). (a) Diurnal temperature lapse rate on Saskatchewan Glacier derived from 5 microloggers installed on ablation stakes from May to August 2015. Mean air temperature LR = -0.463 °C 100 m^{-1} (b) Annual variation of the lapse rate derived from seven weather stations in the study area (see Fig. 1). Mean air temperature LR = -0.495 °C 100 m^{-1}.

Model calibration

Four uncertain model parameters were tuned to improve model fit to observations, the ice albedo, the precipitation correction factor (PCF, %) and the aerodynamic roughness length (*z0*, mm) of ice and snow. An optimized PCF value of 10% was obtained by calibrating the value against end-of-winter snow mass balance observations while the LR value of 14.2% 100 m^{-1}, calculated from the weather station network, was slightly increased to 15% 100 m^{-1} to better fit snow survey observations. An optimized *z0* value of 1.3 mm for ice and 2.85 mm for snow was found by calibrating the model on annual mass balance after correcting the precipitations with the calibrated PCF and LR factors. Optimised z0ice values are in agreement with those reported by Munro (1989) on nearby Peyto Glacier (ice = 0.67 to 2.48 mm, snow = 5 to 6 mm). The albedo was prescribed to 0.3 during other calibration (Gratton et al., 1993; Bordeleau, 1998) and calibrated between 0.2 and 0.6 on ba, with an optimum value of 0.29 found.

Model performance

Comparison with glaciological mass balance

The mass balance simulated with DEBAM was compared with glaciological mass balance observations available between 2012 and 2016. Overall, the seasonal and annual mass balance components are well simulated by the model, with most observations lying near the 1:1 line and with Nash-Sutcliffe Efficiency (NSE, Nash and Sutcliffe, 1970) coefficients of 0.71 for bw, 0.85 for bs and 0.94 for ba for the whole validation period (Fig. 6). Before the adjustment of the atmospheric emissivity calculation in the LWin equation (see section Data and Methods), the results tended to overestimate melt in the accumulation zone and underestimate melt in the ablation zone. The NSE was increased by 0.04 for bw, 0.07 for bs and 0.06 for ba after modifying the parametrisation. The modelled bw was underestimated in 2016 compared to observations in the upper part of the glacier and overestimated in the lower part, suggesting that the precipitation gradient for that year significantly differed from the other years. This shows the limitation of the model, which uses a constant, average precipitation lapse rate to distribute precipitation over the glacier surface. 2016 was a dry year, with the glacier AWS recording a small amount of snow accumulation during winter (AWS: 2015 = 135 cm, 2016 = 25 cm). The NSE for bw improves to 0.84 when excluding the 2016 year. Data from ablation stakes are more limited, and despite the overall good model performance, modelled bs and ba were slightly underestimated in 2014 and 2016 and overestimated in 2015 compared to observation.

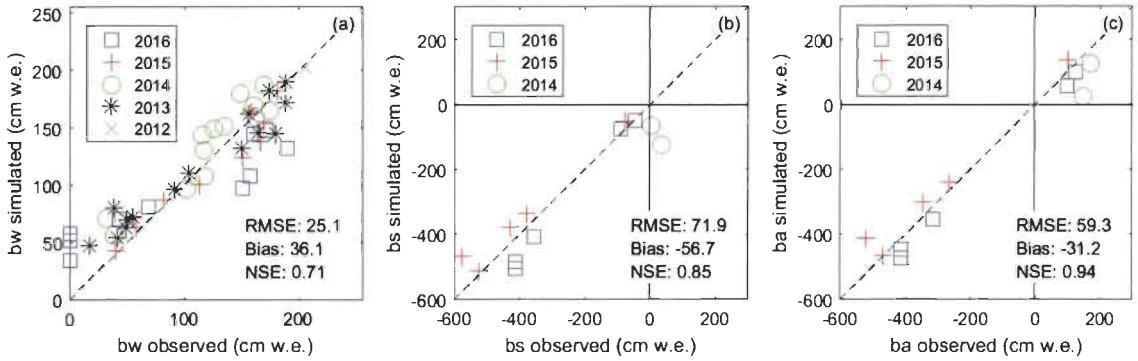

Fig. 6 Simulated mass balance compared with (a) bw, (b) bs, and (c) ba observations between 2012 and 2016. Results are expressed in centimeters water equivalent (cm.w.e.). Dashed line is the 1:1 relationship.

The simulated mass balance gradient compares generally well with observations (Fig. 7). However, the same aforementioned overestimation of ablation at the two ablation stakes available in 2014 is apparent, leading to underestimated mass balance (ba) in the upper glacier that year. The mean mass balance gradient is 0.89 cm.w.e. m^{-1} in the ablation zone and 0.29 cm.w.e. m^{-1} in the accumulation zone. The simulated gradient shows an inflection toward steeper values below the ELA and the observation tend to have the same inflection caused by a steeper part of the glacier with crevasse openings.

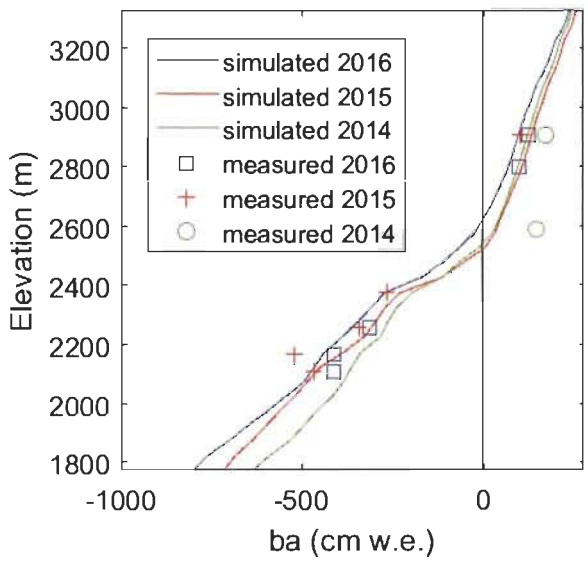

Fig. 7 Simulated annual mass balance gradient compared with measured ba between 2014 and 2016. The symbol and colour scheme are the same as those used in Fig. 6.

Mass balance reconstruction and comparison with geodetics estimates

The cumulative mass balance simulated by the model over the historical period 1979-2016 was compared with the geodetic estimates of Tennant and Menounos (2013) (Fig. 8). The simulated mass balance based on the multi-temporal DEMs (1979; 1986; 1993; 2001; 2009) to account for the dynamical response of the glacier is in line with the geodetic estimates for the earlier period (1979-1993), but diverges after that (1993-2009), the simulated balance being higher than the geodetic estimates but still within its error margins. The error margins around the geodetic estimates are wide, due to the sometimes-large uncertainties in the DEMs. The reported absolute uncertainty was largest for the Shuttle Radar Topographic Mission (SRTM) 2000 DEM (attributed to 1999 to account for radar wave penetration in snow) and for the 2009 DEM derived from the stereoscopy of SPOT satellite images (Tennant and Menounos, 2013). The low contrast of snow in the accumulation area also challenged the calculation of topographic changes and added further uncertainty to the geodetic estimates (Tennant and Menounos, 2013). Static mass balance simulations use a constant glacier geometry over time, i.e. the same glacier DEM for the whole period. As seen in Fig. 8, using the 1979 DEM when glacier extent was maximal results in larger cumulative mass loss than when using the 2009 DEM when glacier extent was at its minimum (~-3 m w.e. over 37 years) because the larger extent in 1979 makes more area available for melting at lower altitudes. The dynamic mass balance simulation remains between the limits of the two endmember static simulations, with a difference in cumulative mass loss of ~ ± 1.4 m w.e at the end of the period.

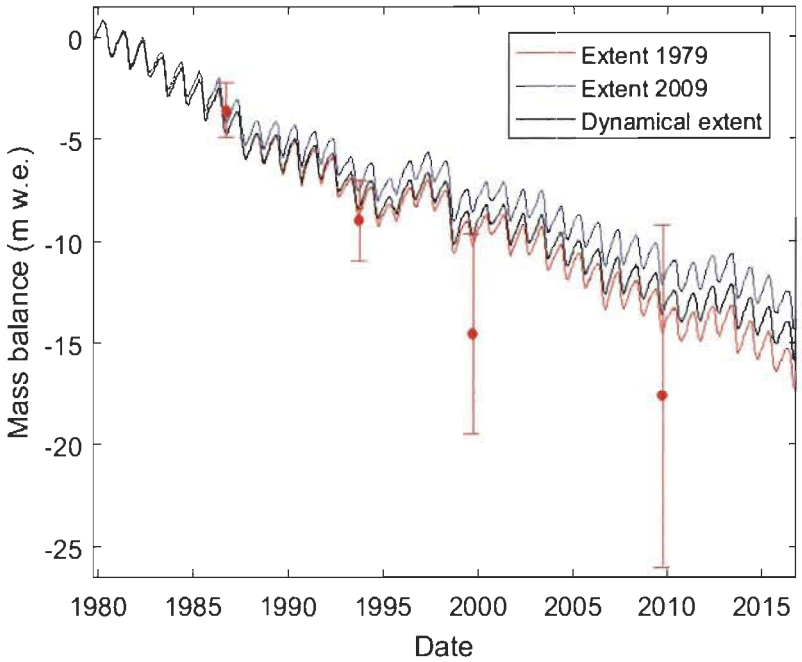

Fig. 8 Simulated cumulative mass balance compared with geodetic estimates from Tennant and Menounos (2013). Error bars represent one-sigma (66%) confidence interval around the cumulative geodetic estimates. The red and blue curves represent static mass balance simulations and the black curve represents the dynamical simulation in which the glacier geometry was updated over time.

The reconstructed glacier-wide mass balance (Ba) of Saskatchewan Glacier was compared with the glaciological record of Peyto Glacier located 70 km southeast from the Columbia Icefield (Fig. 9). In general, Ba variations for both glaciers are relatively synchronous ($R = 0.62$), but lower than theoretically expected given the separation distance between the two glaciers (70 km: $R = 0.80$, Cogley and Adams, 1998). The tendency of both glaciers is however somewhat different. Mean Ba for Peyto for 1979-2016 is -84 cm w.e a^{-1} with a decreasing trend over time, while mean Ba for Saskatchewan Glacier is -47 cm w.e a^{-1}, with more positive balance years than Peyto Glacier and without any clear trend over time. While both glaciers are relatively close, Peyto Glacier is smaller (9 km^2) and its elevation range (2200-3180 m) differs from for Saskatchewan Glacier (23 km^2, 1784-3322 m). The accumulation area of Saskatchewan Glacier thus extends higher than Peyto. The mean accumulation area ratio (AAR) for Saskatchewan Glacier was 0.404 in 2014-15 and 0.459 in 2015-16 (Ednie et al., 2017). For Peyto glacier, the mean AAR for 1966-2017 is 0.34 and near-zero values were

reported for 2013-14, 2014-15 and 2016-17, indicating that the glacier has been completely out of balance with the current climate in recent years (Zemp et al., 2017). Thus, the larger and higher accumulation zone on Saskatchewan Glacier favors accumulation, which partly compensate mass loss on the lower glacier, whereas the shrunken accumulation zone on Peyto Glacier may soon disappear, explaining the accelerating mass loss.

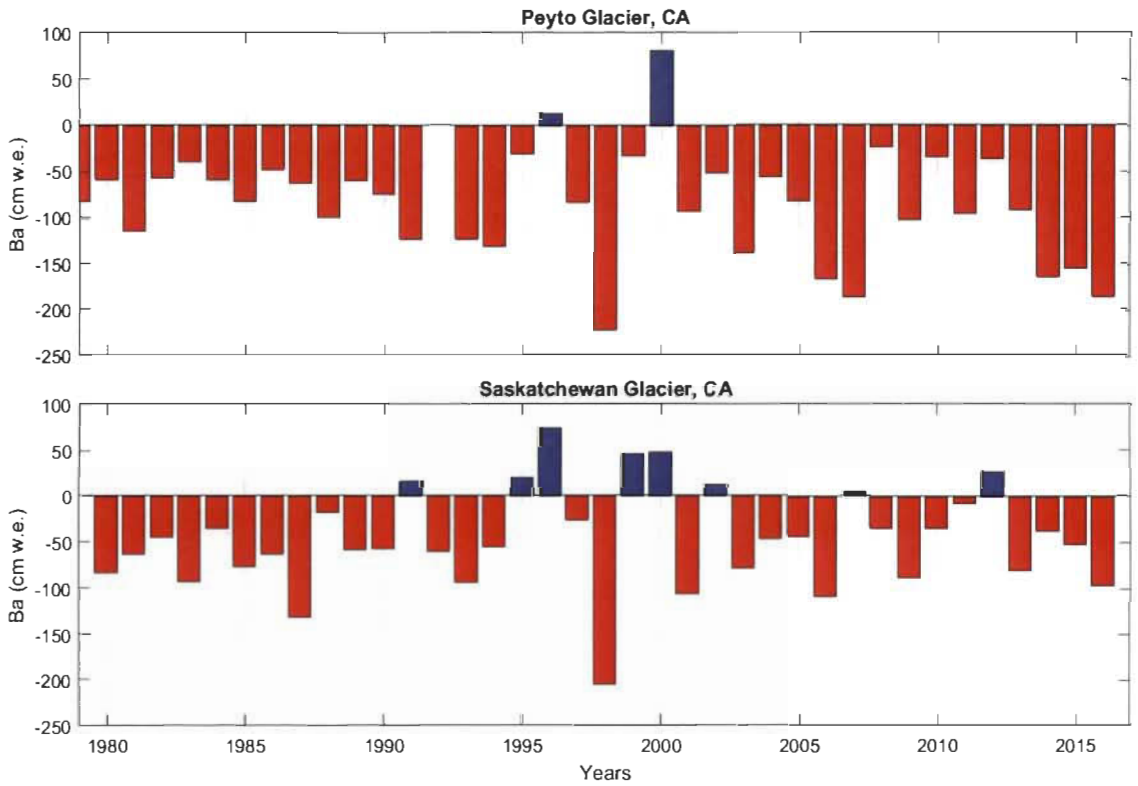

Fig. 9 Annual mass balance of (a) Peyto Glacier as measured by the glaciological method; (b) Saskatchewan Glacier reconstructed from mass balance modelling using 1979 static simulation. Peyto Ba data was extracted from the World Glacier Monitoring Service (WGMS) website while the year 1991 is missing.

Energy and mass fluxes

Temporal and spatial variations in modelled mass and energy fluxes for Saskatchewan Glacier were investigated. The mean energy balance seasonal cycle for the whole glacier shows that the sensible heat flux (QS) dominates energy gains throughout the year (Fig. 10). The contribution of QS is fairly constant throughout the year, increasing

only slightly in July-August and decreasing slightly in spring (March-May). The contribution of the net solar radiation flux (SW*) increases systematically from low values in winter (November-February) when the sun angle is low and the glacier is covered by highly reflective snow, to peak values in July-August when the sun angle is high and low-albedo ice is exposed in the ablation area. Only in July and August does the net solar radiation (SW*) becomes the dominant energy source. The latent heat flux (QL) is small over Saskatchewan Glacier, due to the generally high relative humidity (see Fig. 2). QL is positive on average and highest in summer, reflecting the predominance of deposition and condensation processes over sublimation (see Fig. 12b and Fig. 13b). QL represents a small, but non-negligible (7%) heat gain throughout the year, which reaches 11.5% in July-August. Energy loss occurs mainly by radiative cooling (LW*). Lower air and surface temperature respectively reduce the incoming atmospheric longwave radiation and outgoing longwave emissions from the glacier surface, thereby reducing LW* in winter. LW* increases somewhat in summer (June-August), mainly because the glacier surface is near its melting point, thereby limiting longwave radiation losses. The energy supplied by rain (QR) has a negligible influence on the energy balance. Melting (QM) predominantly occurs between May and October and peaks in July-August, due to the elevated SW*, QS and QL fluxes, and radiative cooling (LWout) limited by the melting surface.

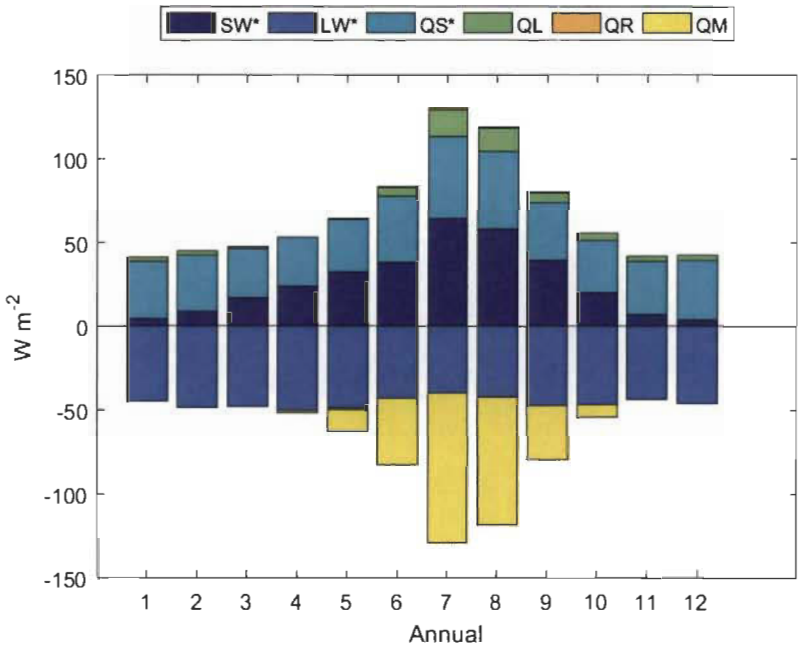

Fig. 10 Mean seasonal cycle of simulated surface energy balance on Saskatchewan Glacier between 1979-2016 using multi-temporal DEM.

Spatial patterns of the surface energy fluxes show variations related to topography, i.e. altitude, slope, aspect and shading. SWin shows the most variations, broadly increasing with altitude due to elevated atmospheric transmissivity, and also on south-facing slopes such as in the northern portion of the glacier (Fig. 11a). Shading effects by surrounding topography are apparent in the southern portion of the glacier tongue and southern upper basin, where radiation values locally decrease. This helps to limit melt at lower altitudes where the albedo is lower (mean annual value of 0.66, Fig. 11b). The higher albedo in the predominantly snow-covered accumulation area counterbalances the larger incoming solar radiation at high elevations. As shown in Fig. 10, LW* is negative, and LWout is on average higher by 46 W m^{-2} than LWin (Fig. 11c, d). Both LWin and LWout are rather uniform, varying spatially by 34 and 27 W m^{-2}, respectively, over the whole glacier. LWin increases towards lower elevations mainly due to warmer air temperatures and some localized contributions from terrain emissions from the surrounding topography on the glacier tongue. Both the latent (QL) and sensible (QH) fluxes decrease with elevation in response to the temperature lapse rate (Fig. 11e, f). The precipitation heat flux increases with elevation due to orographic precipitation and in

response to the precipitation lapse rate prescribed in the model but is otherwise negligible on average.

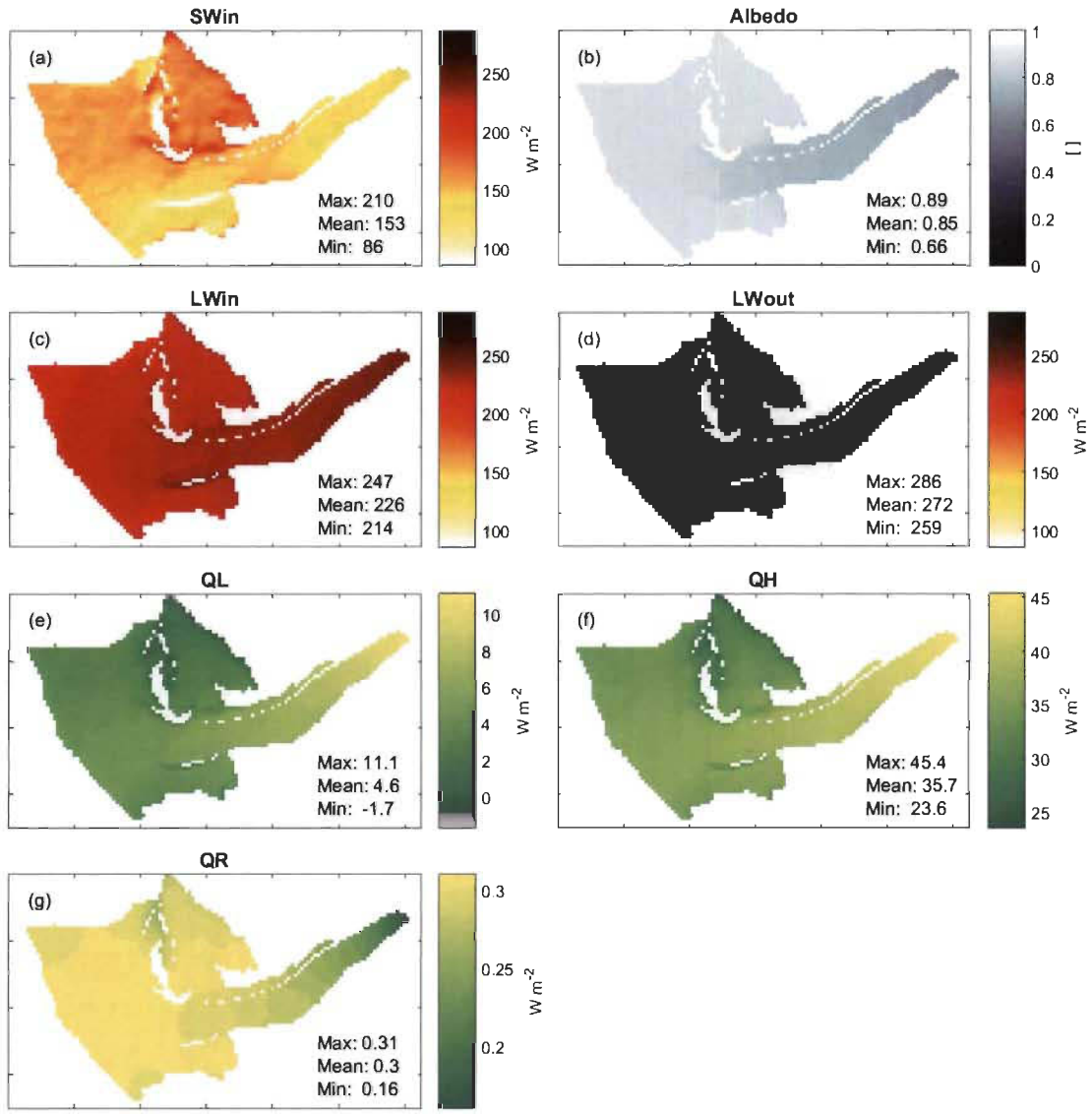

Fig. 11 Mean annual spatial surface energy fluxes simulated on Saskatchewan Glacier between 1979-2016 using 1979 static simulation. Note that the colour scale is common for radiative fluxes (SWin, Lwin and LWout) to ease their comparison.

Four processes influence mass balance during the year (Fig. **12**a). Snow precipitation dominate during the cold season (November-April), leading to snow accumulation during this period. Melt mainly occurs from April to October and

peaks in July-August, in response to the enhanced positive energy balance. Deposition/condensation or sublimation is not visible on Fig. 12a as it does not impact mass balance on a monthly scale. Although the QL heat flux was found to be significant during summer (Fig. 10), the resulting mass loss is itself negligible compared to melting because the latent heat of sublimation/deposition is seven times larger than that for melting. Moreover, the latent heat flux has a pronounced diurnal cycle, switching from deposition at night when cooling of moist air causes the vapour pressure to increase relative to the melting glacier surface, while heating during the days reverses the vapour gradient between the glacier surface and the atmosphere (Fig. 12b). Hence the two regimes tend to compensate each other, but the nighttime deposition slightly dominates daytime sublimation, which leads to a net positive deposition/condensation flux on average to the glacier.

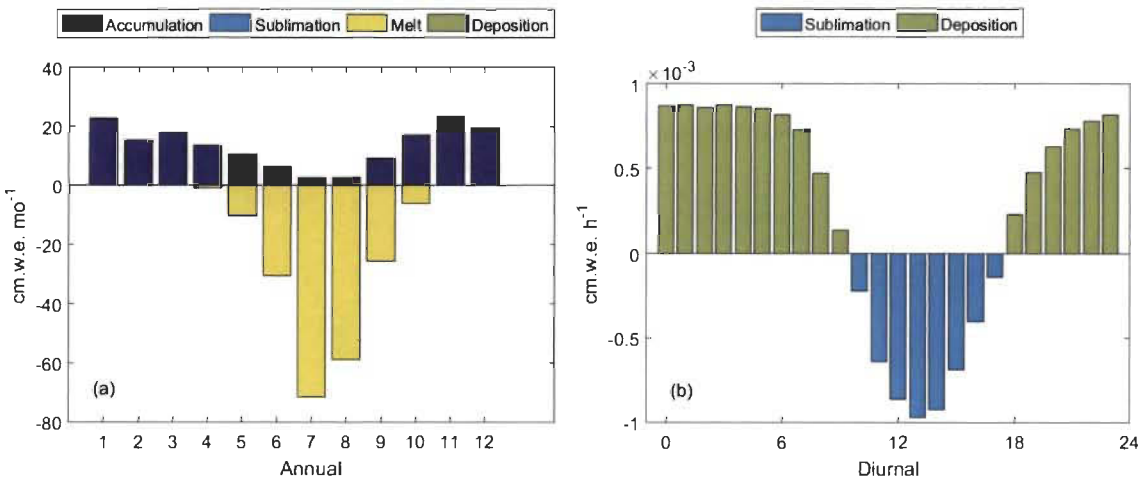

Fig. 12 Mean simulated mass fluxes on Saskatchewan Glacier between 1979-2016 using multi-temporal DEM. (a) Mean monthly fluxes; (b) Mean diurnal cycle in deposition/condensation and sublimation.

Spatial mass balance patterns (Fig. 13) show an annual snowfall average of 159 cm w.e over all the glacier with a minimum of 30 cm w.e near the front to ~300 cm w.e. in the highest part of the glacier. The precipitation LR was recalculated after the mass balance simulation on spatial mean snow precipitation grid of 1979-2016. The variation show a smoother LR (11%/100m) than the prescribed precipitation LR of 15%/100 m. Annual ice melt can reach 787 cm w.e. at the glacier margin and 53 cm w.e. in the upper

accumulation zone. Deposition/condensation predominates on average over the glacier but fluxes are small (< 4 cm w.e. a^{-1}), and limited sublimation only occurs in the upper reaches of the glacier (Fig. 13c). On average, melting (-208 cm w.e. a^{-1}) dominates snow precipitation (+159 cm w.e. a^{-1}) and the small deposition gain (+2 cm w.e. a^{-1}), yielding a mean negative annual balance (-47 cm w.e. a^{-1}).

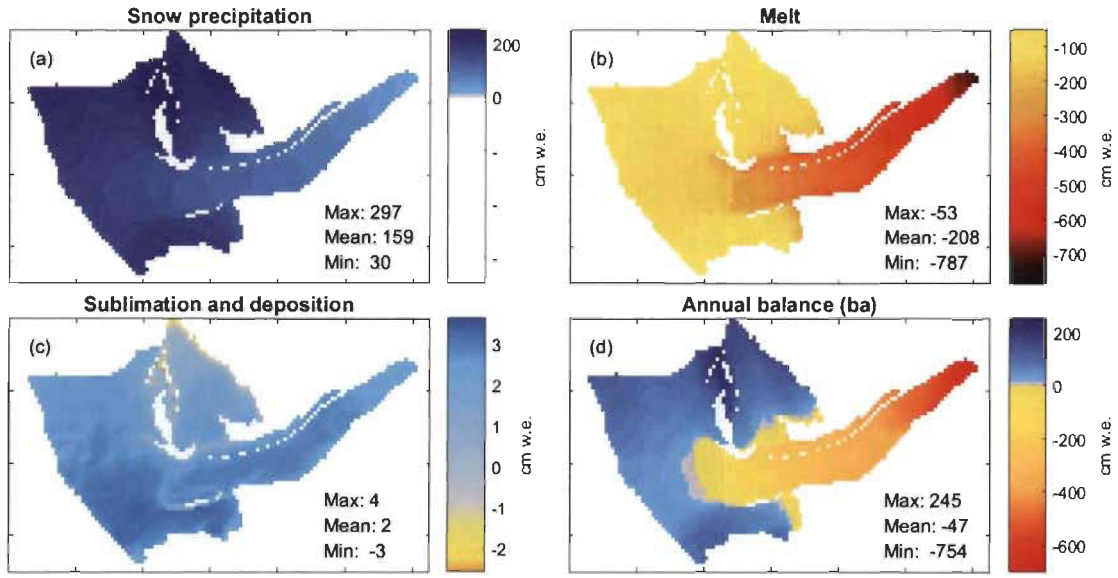

Fig. 13 Simulated spatial patterns of annual mass balance in cm w.e. on Saskatchewan Glacier between 1979-2016 using 1979 static simulation: (a) snow precipitation; (b) melt; (c) sublimation and deposition; (d) annual balance. The accumulation zone is represented in blue, the ablation zone is represented in yellow/red while the grey is the equilibrium line (ba = 0).

Climate sensitivity analysis

The static sensitivity of mean mass balance components to various climate perturbations (ΔTa = 0 to +8 °C and ΔP= -20 to +20%), using the GLIMS extent with 2010 DEM as reference glacier geometry, is displayed as response surfaces in Fig. 14. The reference scenario gives an average annual mass loss (Ba) of -0.49 m w.e. a^{-1} (Fig. 14c). The response surface for Ba shows that the glacier-wide mass balance is overall very sensitive to changes in air temperature, and much less sensitive to changes in precipitation, as seen from the Δba contours oriented almost vertically on Fig. 14c. The ΔBa contours also become steeper and narrower with increased warming, which

indicates a reduced sensitivity to precipitation and increased sensitivity to temperature with warming, respectively. The seasonal mass balance response sufaces help to understand the Ba sensitivities (Fig. 14a, b). First, it can be seen that a precipitation increase of +20% can buffer the negative impact of warming on Bw up to +3 °C of warming and then that a warming of more than +6 °C with no change in precipitation would completely eliminate the accumulation zone of the glacier, given the current glacier extent (2009) (Fig. 14a). The sensitivity of winter mass balance to temperature changes also increases markedly with warming, as seen by the progresive tightening of contours on Fig. 14a. This is interpreted to result from reduced accumulation due to a reduced snowfall fraction, as well as increased ablation during winter (Oct.-April) due to earlier disapearance of the snow cover under more pronouced warming. On the other hand the temperature sensitivity of summer mass balance (Bs) does not change signficantly with the warming scenario, and the steep contours on Fig. 14b indicated a small sensitivity to precipitation changes. Hence, summer accumulation and albedo feedbacks on summer (May-Sept.) ablation appear to be small, and the increased temperature sensitivity of Ba with warming seen on Fig. 14c is rather attributed to decreasing accumulation from reduced snowfall fraction and increased winter ablation as climate warms (Fig. 14a).

IPCC RCP scenarios +2.6, +4.5, +6.0 and +8.5 for the mid (2046-2065) and late (2081-2100) 21st century overlapped onto the response surfaces show the most likely future climate trajectories given by the latest projections from climate models. The RCP projection have significant uncertainities, as shown by their wide 5-95% confidence intervals (e.g. late-century RCP +6.0: ΔT = 1.7 to 5 °C and ΔP = -4 to 18.6%), and the annual mass balance change can vary by as much as ±3 m.w.e. a^{-1} within a single scenario. This illustrates the usefulness of scenario-free response surfaces to assess glacier mass balance sensitivity to climate as a background to evolving climate projections (Prudhomme et al., 2010). Nontheless, given the current scenarios the (static) mass balance could decrease by -1 to -2.5 m w.e a^{-1} by the mid-century, and by -1 to -4 m w.e a^{-1} at the end of the century, relative to baseline conditions (Ba = -0.49 m w.e. a^{-1}) and depending on the RCP scenario considered.

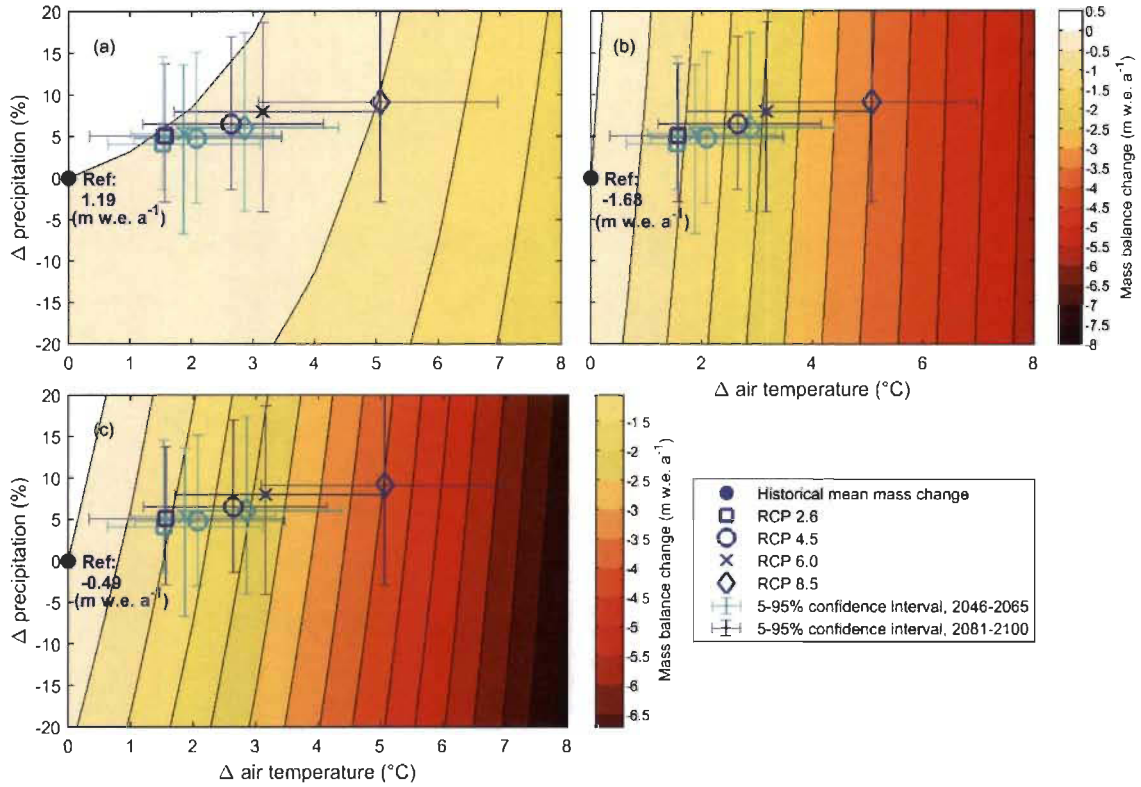

Fig. 14 Static mass balance sensitivity (reference periods of 1981-2000, DEM 2010) to prescribed changes in regional mean air temperature between 0 to 8 °C and precipitation between -20 to +20%, which comprises IPCC representative concentration pathways (RCP) scenarios +2.6, +4.5, +6.0 and +8.5 including 5-95% confidence interval for the mid (2046-2065) and late (2081-2100) 21st century. (a) Winter balance (Bw). (b) Summer balance (Bs). (c) Annual balance (Ba).

As Ba display a large sensitivity to temperature and because glacier melt is the outcome of complex glacier-atmosphere energy exchanges, the sensitvity of energy balance to warming was further investigated (Fig. 15). The total energy input to the glacier surface increases with rising temperatures, and the increased energy is predominantly used for melting (QM) (Fig. 15b: ΔQ = -6.1 W m^{-2} after a 1 °C perturbation). Interestingly, the increase in energy supply with warming is mainly driven by an increase in net solar radiation (SW*) (ΔQ + 1 °C = 3.01 W m^{-2}) and latent heat flux (QL) (ΔQ + 1 °C = 1.5 W m^{-2}), with more subdued increases in sensible heat flux (QS) (ΔQ + 1 °C = 1.3 W m^{-2}) and net longwave radiation fluxes (LW*) (Fig. 15b). Since cloud cover is unaffected by the temperature perturbations, the increase in SW* with warming is entirely driven by the decreasing albedo as snow cover duration on the glacier decreases in

response to warming. Since the relative humidity remains unchanged in our sensitivity tests and warming causes the air saturated vapor pressure to increase, warming will then result in increased atmospheric vapor pressure. Because the glacier surface is contrained to the melting temperature (0 °C) during a long part of the year, the increase in surface saturated vapor pressure in response to warming will be less than that of the atmosphere, causing the vapor pressure gradient to increase and boost QL fluxes (deposition) to the surface. Similar reasoning applies to QS, i.e. the near surface temperature gradient will increase in response to atmospheric warming while the warming of the glacier surface is limited by melting.

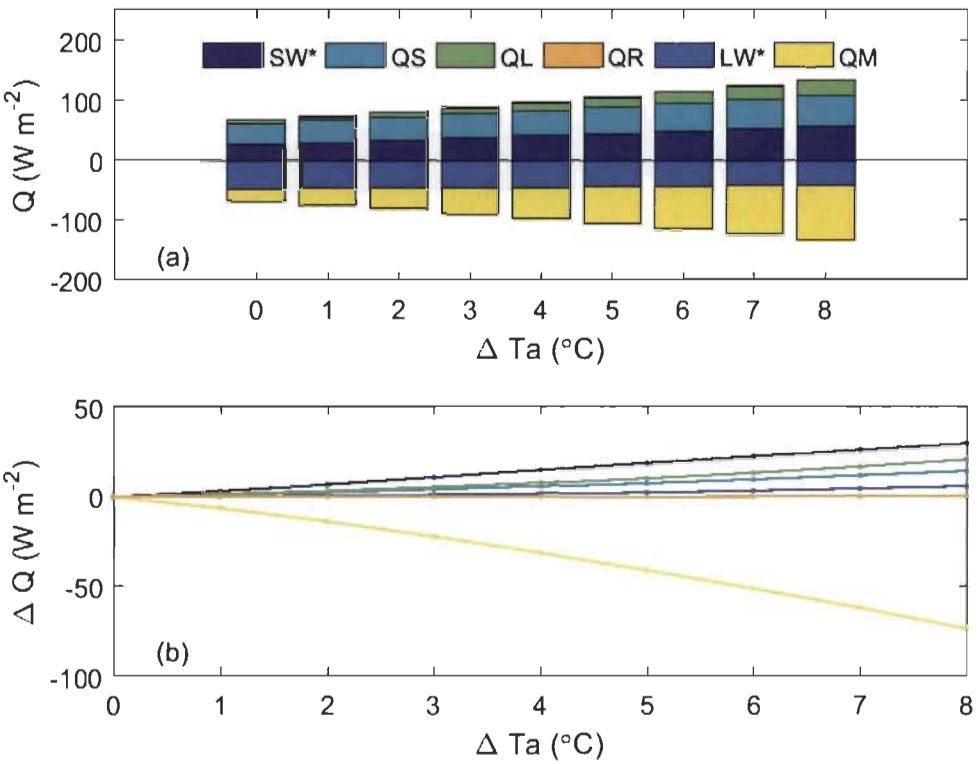

Fig. 15 Static energy-balance sensitivity to changes in regional mean air temperature between 0 to 8 °C. (a) Energy balance for each synthetic warming scenario; (b) Change in energy flux relative to reference period (1981-2000).

Discussion and conclusion

Downscaling NARR with scarce glacier observations

The present study focused on reconstructing the mass balance of a glacier using a physically based model and a sparse set of glacio-meteorological data. This situation is common to many mountain glaciers of the world where logistical and financial constrains preclude long and continuous monitoring programs. NARR is a long-term, consistent climate dataset with a high spatial (32 km) and temporal (3-hourly) resolution that has proven its accuracy especially with 2 m temperature and 10 m wind in comparison with other global reanalysis datasets (Mesinger et al., 2006), and also precipitation (Choi et al., 2009; Essou et al., 2016). In our study, the use of downscaled NARR data (Ebrahimi and Marshall, 2016; Clarke et al., 2015) was an convenient way to generate inputs to DEBAM, and the comparison between NARR and observations was reasonably good given the short AWS record used for comparison. Even without downscaling, three variables (Ta, RH, SWin) showed good correlation ($R > 0.85$) between NARR and AWS observations, and the simple scaling bias correction applied removed much of the biases present.

Choi et al. (2009) reported an average correlation (R) of 0.98 for temperature and an RMSE of 3.2 °C without downscale for six weather stations spread across Manitoba. In our study the R value was 0.98 before downscale with an RMSE of 1.94 °C (decreasing to 1.49 °C after downscaling). However, it should be considered that their statistics include the entire period from 1979 to 2004 while our temperature statistics at the AWS include only 2 years. Their study also revealed a warm bias of about 2 °C for NARR, while the cold bias of -1.26 °C observed in our study can be almost entirely explained by the difference in elevation of 237 m between the NARR gridpoint (2430 m a.s.l.) and AWS (2193 m a.s.l.). Using the mean calculated lapse rate (-0.463 °C 100 m^{-1}), the difference of elevation can explain -1.1 °C, which lead to a cold bias of -0.16 °C in NARR. The comparison between NARR and observations in our study is thus good, but it is important to keep in mind the difference in time frame between the two studies, but also the difference in topography when comparing the Canadian Rockies with the Manitoba plains. To avoid most of the altitude biases in the Canadian Rockies, Ebrahimi

and Marshall (2016) applied a perturbation approach of daily weather anomalies on every NARR daily meteorological fields relative to the mean NARR condition of the weather station period. In our case, we used a similar method only for SWin, while temperature was downscaled with a simple scaling method, which gave good results. For comparison purpose with all our variables, Rye et al. (2010) worked on a glacier in northwestern Svalbard and found a correlation of 0.93 between observed and downscaled ERA-40 reanalyses air temperature (~125 km spatial resolution) using the EQM method with 3 times daily observations since 1969. On the other hand, SWin is strongly correlated (R = 0.92) due to the seasonal and diurnal cycle compared to Rye et al. (2010) who found a daily mean correlation of 0.61. Despite the good correlation, the RMSE remains very high (53 to 39 W m^2), even after applying the monthly mean diurnal multiplicative correction factor. NARR seems to have a problem with the representativeness of the inter-annual variance of radiation fluxes, as demonstrated by Ebrahimi and Marshall (2016) even though the correlation of incoming shortwave radiation fluxes between 11 years of AWS summer (JJA) data and the NARR gridpoint remains moderately strong for their study (R=0.50). Thus, we agree with their suggestion that more studies are needed to elucidate the poor representation of radiation fluxes and cloud cover in the NARR in mountainous region and their ability to simulate energy and mass balance. Surprisingly, the RH daily mean correlation is very high between NARR and observations with R = 0.85 compared to R = 0.41 for Rye et al. (2010), making it his weakest relationship of the climate variables. Wind speed (WS) was however poorly represented with a daily mean correlation of 0.37, while Rye et al. (2010) have a daily mean correlation of 0.64. The higher resolution of the NARR product (32 km) could explain the better correlations found in this work compared to the coarser ERA40 reanalyses (125 km) used by Rye et al. (2010). The correlation between observed and NARR daily wind speed was weak compared to Ta and RH (R = 0.37). We suspect that this arises because the thermal winds (katabatic and valley winds) are not represented at the coarse 32 × 32 km spatial resolution of the NARR (Dadic et al., 2010).

The NARR gridpoint is also 430 m higher than the homogenized historical precipitation record elevation (mean: 2002 m a.s.l.). The bias in NARR relative to the

observed precipitation (0.55 mm d^{-1}) is less than that expected from the elevation difference when using the mean lapse rape of 15%/100m used in the model, which predicts a positive bias of 1.05 mm d^{-1}. However, the mean winter lapse rate was used in the model, which is steeper than the mean annual lapse rate. Its is plausible then that the elevation difference may explain most of the observed bias in the raw NARR precipitation. The poor correlation of NARR precipitation with the off-glacier homogenized historical precipitation record (R = 0.30) is also similar to the study of Ebrahimi and Marshall (2016) who found that the NARR poorly represented the observed winter accumulation totals. The simple scaling used for bias correction reduced the first order bias in the NARR precipitation but did not resolve all errors, and more elaborate downscaling would be desirable for future studies. Again, Choi et al. (2009) reported an average R of 0.62 for daily precipitation and an RMSE of 3.4 mm d^{-1} without downscale for six stations spread across Manitoba compared to our study before the downscale with an R of 0.30 and an RMSE of 5.22 mm d^{-1} (poor upgrade to 4.96 mm d^{-1} after downscaling). This time, our statistics were made with a long period of 334 months between 1960 and 2005 which is directly comparable with Choi et al. (2009). The R values are much lower than temperature, so it supposed that even on a flat surface (< 400 m difference between the 6 stations in Choi et al. (2009)) the precipitation is hard to simulate. Their study also showed the inability of weather data and reanalysis data to correctly locate a precipitation event in time, where large positive error are immediately followed by large negative errors with similar magnitude or vice versa (Choi et al., 2009). Following the same pattern, a study in Alberta's plains showed an underestimation of the maximum values of precipitation while overestimating the cumulative annual precipitation of the NARR in some years (Keshta and Elshorbagy, 2011). Again, for comparison purposes with another reanalysis products, Rye et al. (2010) obtained a daily correlation coefficient of 0.53 and a part of this result is explained by substantial errors of snowfall measurements on high wind and low temperature at precipitation gauge. Also, many studies show that improving the spatial resolution also improves the representation of local climatic features, especially in mountainous fields with precipitation (Erler et al., 2015; Rasmussen et al., 2011; Pollock and Bush, 2013; Mesinger et al., 2006). Thus, working with incomplete AWS data requires filling the gaps with alternative sources, and NARR remains the best current

option in our case that is available everywhere in North America at an acceptable resolution. The performance of statistical downscaling with a simple predictor (the 'direct method') is the most straightforward to implement and can show better results in the case of temperature than using a multivariate predictor approach with different gridpoints, vertical levels ad other predictor variables (Hofer et al., 2017). However, Hofer et al. (2017) suggest that the use of multivariate predictors performs better in general, particularly for wind, which should be considered in future analyses. Precipitation is also the variable who show the lowest skill in Hofer et al. (2017).

Finally, it is worth noting that data gaps in June 2015 and 2016 due to the AWS falling down resulted in data loss during crucial high-melt periods, which could have impacted the calibration of the bias correction functions. Still, these gaps represented only 3% of the period so that their overall effect is presumably small.

Model performance

The results obtained by comparing the direct mass balance observations with the DEBAM simulations over a period of 3 to 5 years showed that the model performs generally well, with NSE values from 0.71 to 0.94 (Fig. 6). In addition, the interannual variability in mass balance was relatively well simulated by the model despite the constant precipitation lapse rates used in the model. However, simulated bw values in 2016 deviate from the rest of the data and may reflect the limitation of using a constant precipitation lapse rate. Point mass balance observations using the glaciological method are affected by uncertainties related to the errors in ablation stake height measurements, stake sinking into the ice or firn and snow/firn density measurements, while glacier-wide (mean) mass balance is further impacted by sampling errors, i.e. spatial mass balance variability not captured by the stake and snowpit network (Zemp et al., 2013). Errors in glaciological measurements are generally higher for bs (-25 to +40 cm w.e. in the accumulation area) than for bw (-10 to +15 cm w.e. for ablation and accumulation area or -30 to +15 cm w.e. for snow probing in ablation area). The accumulation area is also more favourable to larger errors compared to ablation zone (i.e. the hard layer that marks the end of the melt season

is always used to calculate bw in the ablation zone; more refreezing in the snowpack into the accumulation zone) (Gerbaux et al., 2005). The cumulative errors at point stakes can be important over the years and can range from 14 cm w.e. a^{-1} for ablation measurements on ice, 27 cm w.e. a^{-1} for ablation measurements on firn and 21 cm w.e. a^{-1} for snow measurements in the accumulation area (Thibert et al., 2008). The RMSE on bw simulated by the model is 25.1 cm w.e. a^{-1}, on the same order as the typical error for snow and firn, thus affirming that the accuracy of the model is good (Fig. 6).

A poorer comparison was observed between the simulated mass balance and the geodetic estimates from Tennant and Menounos (2013) over the 1979-2016 period (Fig. 8). Potential sources of errors that can explain this discrepancy include systematic and random errors in the glaciological and geodetic mass balance estimates, as well as structural errors of the models. Thibert et al. (2008) recommended using photogrammetric measurements to avoid and correct for the annual accumulation of systematic errors in long glaciological mass balance observations records. Random and systematic errors are still present with the geodetic method, but comparing two DEMs over several years results in a lower error in mass balance annual rates. However, the method used by Tennant and Menounos (2013) on Columbia Icefields consisted in comparing 5 DEM successively over 4 periods i.e. 1979-86, 1986-93, etc. Random and systematic errors are thus accumulated at each period and lead to errors of up to 8.37 m w.e. after 4 periods spread over 30 years, which is close to the error of the glaciological method with 28 cm w.e. a^{-1}. The wide error bars on the cumulative geodetic balance (Fig. 8) reflect the accumulation of systematic errors as estimated on stable ground between each DEM and a 1986 reference DEM, random relative errors estimated on stable ground between each successive DEM, an error term for changes in firn and an error term for missing data in the low-contrast accumulation zone. This last term, estimated at ± 5 m.w.e., suggests that the geodetic estimates are biased toward the higher-contrast ablation zone of the glacier, resulting in an overestimation of mass loss for the whole glacier. This error could have been reduced to about 6.6 cm w.e. a^{-1} by directly comparing all DEMs to a reference DEM (e.g. 1979). The wide confidence interval of the geodetic estimates is an important issue of the validation.

Another source of uncertainty is the long-term representativity of the NARR (Fig. 4). The quality of the dataset directly impacts the mass balance simulations, especially outside of the AWS period used for the downscaling. Still, several studies recommend the use of NARR in hydrological model with flat topography, particularly when the data are sparse in order to fill the gaps of AWS data (Choi et al., 2009; Keshta and Elshorbagy, 2011). The poor representation of cloud cover and radiation fluxes requires further study since it can reduce the skill of NARR to simulate mass and energy balance reconstructions (Ebrahimi and Marshall, 2016).

Finally, it is possible that uncertain model parameters, either those calibrated on the mass balance and meteorological observations or prescribed from observations (e.g, fixed albedo values, lapse rates), do not adequately represent the entire historical period. The precipitation gradient set at 15% 100 m^{-1} will vary over time (e.g. Fig. 6), as well as the albedo values of snow and ice that also remain fixed over time in our model. Decreasing snow and ice albedo typically occurs over the course of the melt-season as the snow ages and impurities concentrate at the surface (Cuffey and Paterson, 2010), but also due to by more discrete events not taken into account in our modeling such as algal mat development (Lutz et al., 2014; Takeuchi et al., 2001) or wildfire that bring impurities on the glacier and affect albedo (Wang et al., 2016; Kim et al., 2005). Long-term darkening has also been observed on glaciers of the Alps, which question the use of fixed albedo values in historical mass balance simulations (Oerlemans et al., 2009).

Impact of glacier movement

The multi-temporal DEMs used in the study allowed the precise delineation of the glacier surface to understand the impact of glacier movement on long-term mass balance (Fig. 8). In total only ~3 m w.e. over 37 years differs between the mass balance simulations with the two static DEMs of 1979 and 2009, with that the dynamic mass balance (dynamical extent, black line) being located between the two extreme scenarios (1979, 2009). The difference between the static and dynamic mass balance is less than or equivalent to the average error of the geodetic mass balance of Tennant and Menounos

(2013). In addition, the current topography is suitable for melting since the glacier margin is at the bottom of the valley and glacial retreat currently occurs over a restricted altitude range, limiting any negative feedback of glacier retreat on mass balance. When the glacier will retreat to higher elevations, there will be a reduction of melt due to lower temperatures. It will gradually increase the difference between the static balance and the one that constantly adapts its geometry (Huss et al., 2012). The dynamic adjustment was evaluated on the historical period while the climate sensitivity analysis was performed with the static extent of 2009, making the results of sensitivity analysis somewhat more pessimistic than the reality. We know that dynamic adjustment is less sensitive on a long period of time, especially if the glacier size is not in equilibrium with the historical climate of about 30 years ago. If the glacier is in equilibrium with the climate, the static mass balance simulation will be less sensitive (Oerlemans et al., 1998), which is not the case in RCP climate scenarios projected for 2100. An interesting analysis would be to add the Volume-Area scaling in the sensitivity analysis in order to see the effect of the dynamic adjustment to the late-century RCP scenarios.

Climate sensitivity analysis

Mass balance is clearly most sensitive to air temperature as shown with the almost-vertical response surfaces on Bs and Ba (Fig. 14b, c), while the change in precipitation (ΔP) primarily affects Bw with a small proportion (Fig. 14a). Our climate sensitivity analysis showed that an increase in precipitation of 20% can compensate the decrease in Bw in response to a warming of up to 3 °C (Fig. 14a). Previous works on mass balance sensitivity to climate have shown that glaciers in wetter climates are more sensitive to air temperature change, and that plausible or projected increases in precipitation are not sufficient to compensate for the increase melting in a warmer climate (Oerlemans and Fortuin, 1992). After this threshold, the majority of the precipitation fall as rain and snow accumulation ceases. Peyto Glacier is located in a dry continental climate (Demuth and Pietroniro, 1999) and Saskatchewan Glacier is located in a similar environment (50 km away from Peyto) which should somewhat make it less sensitive to air temperature change and more sensitive to precipitation then maritime glacier. A warming of 1 °C leads to an

annual change in ΔQM of -6.1 W m^{-2} (-0.58 m w.e. a^{-1}) (Fig. 15) which also leads to a more negative Ba (ΔBa = -0.62 m w.e. a^{-1}) compared to the 1981-2000 reference period (Fig. 14c). Using the annual precipitation (874 mm a^{-1}) of downscaled NARR and the mass balance sensitivity to temperature (-0.62 m w.e. a^{-1}), we can see that our simulation is too responsive compared to glaciers in a similar climate and the same amount of precipitation (between ~ -0.35 to -0.5 m w.e. a^{-1}) (Cuffey and Paterson, 2010, p. 106). However, the difference is not significant considering the variability of sensitivities in many similar studies on high-latitude glaciers (>60°N) ranging from -0.1 to -2 m w.e. a^{-1} (De Woul and Hock, 2005). On the other hand, a rise of 10% of the precipitation leads to an increase in ΔBa of +0.19 m. w.e. a^{-1}, while the same studies range mostly between 0.1 to +0.4 m w.e. a^{-1} (De Woul and Hock, 2005). A comparison of the sensitivity of the Saskatchewan Glacier with maritime and continental glaciers shows that it is somewhere in the average, and that its sensitivity is considerably lower than for maritime glaciers. Continental glacier need a much higher percentage increase of precipitation to balance the effects of a temperature increase beacause of a higher annual temperature amplitudes that affects the snow and rain precipitation fraction (De Woul and Hock, 2005).

Climate change poses a challenge for glacier mass balance empirical models because they are used for projection of significantly different conditions (Refsgaard et al., 2014). Physically based models rely on energy-balance calculations to explicitly account for all energy exchanges between the glacier surface and atmosphere. These models better represent the physical processes which drive glacier ablation (Fig. 15) and are thus more transferable over time (MacDougall and Flowers, 2011). Several studies used energy-balance model to perform sensitivity analysis in order to reproduce future climatic scenarios of temperature and precipitation (Oerlemans and Fortuin, 1992; Hock et al., 2005; Anslow et al., 2008; Anderson et al., 2010), but also to see the impact of parameters calibration and transferability on mass balance, e.g. aerodynamic roughness lengths (z0) , wind, albedo, etc. (Ebrahimi and Marshall, 2016; Réveillet et al., 2017a). We agree to the conclusions reach by these authors, that not only temperature and precipitation can have a major effect on the mass balance of a glacier. Even though we have calibrated ice z0 and albedo as well as temperature and precipitation LR according to observations or logical

values from the literature, we did not focus on the sensitivity analysis of these parameters on mass balance. For example, Ebrahimi and Marshall (2016) reported a perturbation in energy balance higher than 100 W m^{-2} at local noon in mid-summer for an increase of 0.1 in the ice albedo on Haig Glacier, also in the Canadian Rocky Mountains. As this glacier has a climate environment similar to that of Saskatchewan Glacier, we can expect albedo to be a very sensitive parameter that can vary in time and spatially with the darkening process, e.g. algal mat development (Lutz et al., 2014; Takeuchi et al., 2001) or wildfire impurities (Wang et al., 2016; Kim et al., 2005). An interesting study analysing glacier response time and sensitivity to ELA change showed that the volume sensitivity is more related to the glacier size distribution while the glacier response time is mostly driven by the climatic settings (Bach et al., 2018). In our case, it means that the configuration of the DEM does not have a big influence on the glacier response to precipitation and temperature changes. Even with the GLIMS extent used for the sensitivity analysis instead of TM extent used for the static and dynamical analysis, the pattern of the sensitivity will stay the same.

Conclusion

In conclusion, the framework proposed here follow the pioneering work on climate sensitivity by Oerlemans and Fortuin (1992) using a physically based, distributed glacier mass balance model DEBAM (Hock and Holmgren, 2005) forced with 1979-2016 downscaled NARR data (Mesinger et al., 2006; Ebrahimi and Marshall, 2016). Even with short, scarce *insitu* AWS and glaciological data to perform downscaling and calibration, the simulated mass balance corresponds well with observations from 2012-2016. The simulated cumulative mass balance is smaller than, but within the error margins of, the geodetic estimates of Tennant and Menounos (2013) and the reconstructed annual mass balance shows similarity with Peyto glacier record but does not show an acceleration toward more negative balance as seen for Peyto. The ablation is dominated by melt with negligible sublimation losses and deposition gains. Melt varies between 1 m and more than 7 m w.e. a^{-1} near the margin. We also revealed that the impact of glacier retreat on mass balance was small over the historical 1979-2016 period, with a difference between

static extent (1979 and 2009) and a dynamical extent simulation being less than 1.4 m w.e. over 37 years. Finally, we show that the mass balance of Saskatchewan is mostly sensitive to air temperature, with comparatively lower sensitivity to precipitation. Plausible increase in precipitation up to +20% are not sufficient to compensate the impact of warming air temperature on Ba. The actual 1981-2000 reference period Ba is -0.49 m w.e. per year and could further decrease by an additional -1.2 m w.e. a^{-1} for 2046-65 and by about -2 m w.e. a^{-1} for 2081-2100 under scenario RCP +6.0.

Appendices

Table S1: Additional statistics about the four different downscaling methods (No downscale, Scaling, Delta, EQM): The calibration statistics consist on comparing the whole AWS data with NARR on (a) hourly and (b) daily time step. The validation statistics consist to split the AWS data into two sub-period, proceeding on a cross sample validation and taking the mean value of the two series on (c) hourly and (d) daily time step.

	Method	Statistic	Ta (°C)	WS ($m\ s^{-1}$)	RH (%)	SWin ($W\ m^{-2}$)	P ($mm\ d^{-1}$)
(a)	No downscale	Pearson	**0.96**	0.26	**0.77**	0.91	-
		RMSE	2.57	**2.90**	**11.12**	111.55	-
		Bias	-1.26	-1.11	-0.11	29.76	-
		MAE	1.98	2.31	8.52	61.00	-
	Scaling	Pearson	0.96	0.26	0.77	**0.92**	-
		RMSE	2.25	**2.90**	11.13	**97.64**	-
		Bias	0.00	0.00	0.00	**-0.14**	-
		MAE	1.71	**2.28**	**8.50**	**47.05**	-
	Delta	Pearson	0.96	**0.27**	0.77	-	-
		RMSE	**2.04**	3.15	11.45	-	-
		Bias	0.00	0.00	0.00	-	-
		MAE	**1.55**	2.47	8.55	-	-
	EQM	Pearson	0.96	**0.27**	0.77	-	-
		RMSE	**2.04**	3.15	11.48	-	-
		Bias	0.02	0.00	-0.02	-	-
		MAE	**1.55**	2.47	8.59	-	-
(b)	No downscale	Pearson	**0.98**	**0.37**	0.85	0.92	0.30
		RMSE	1.94	2.30	7.96	52.98	5.22
		Bias	-1.26	-1.11	-0.09	30.30	0.55
		MAE	1.57	1.85	6.16	38.58	3.10
	Scaling	Pearson	0.98	0.37	0.85	**0.93**	**0.53**
		RMSE	1.48	**2.13**	**7.96**	**37.11**	**4.19**
		Bias	0.00	0.00	0.02	0.32	0.00
		MAE	1.15	**1.66**	6.14	**27.20**	**2.35**
	Delta	Pearson	0.98	0.37	**0.86**	-	0.52
		RMSE	**1.34**	2.28	7.98	-	4.83
		Bias	0.00	0.01	0.02	-	0.00
		MAE	**1.01**	1.78	**5.97**	-	2.43
	EQM	Pearson	0.98	0.37	**0.86**	-	0.52
		RMSE	1.35	2.27	8.00	-	4.76
		Bias	0.01	0.00	**0.00**	-	-0.04

	Method	Statistic	Ta (°C)	WS ($m\ s^{-1}$)	RH (%)	SWin ($W\ m^{-2}$)	P ($mm\ d^{-1}$)
		MAE	**1.01**	1.77	5.98	-	2.41
(c)	No downscale	Pearson	**0.95**	0.26	**0.76**	0.91	-
		RMSE	2.57	**2.90**	**11.12**	111.17	-
		Bias	-1.26	-1.13	-0.11	29.94	-
		MAE	1.99	**2.32**	8.52	60.84	-
	Scaling	Pearson	0.95	0.26	**0.76**	**0.92**	-
		RMSE	2.25	2.96	11.13	**101.08**	-
		Bias	**0.00**	-0.01	**0.00**	**-0.74**	-
		MAE	1.72	2.33	**8.51**	**48.60**	-
	Delta	Pearson	0.95	**0.27**	**0.76**	-	-
		RMSE	2.52	3.19	11.89	-	-
		Bias	**0.00**	-0.01	**0.00**	-	-
		MAE	1.83	2.50	8.90	-	-
	EQM	Pearson	0.95	**0.27**	0.77	-	-
		RMSE	**2.08**	3.18	11.57	-	-
		Bias	0.03	**0.00**	-0.13	-	-
		MAE	**1.58**	2.50	8.68	-	-
(d)	No downscale	Pearson	**0.98**	**0.37**	0.85	0.92	0.30
		RMSE	1.94	2.30	**7.96**	52.72	5.22
		Bias	-1.26	-1.12	-0.09	30.41	0.55
		MAE	1.57	1.85	6.17	38.51	3.10
	Scaling	Pearson	0.98	0.37	0.85	**0.93**	**0.30**
		RMSE	1.49	**2.21**	7.97	**39.08**	**4.96**
		Bias	**0.00**	**0.00**	0.03	**-0.25**	**0.0**
		MAE	1.16	**1.72**	6.15	**29.10**	**2.82**
	Delta	Pearson	0.97	0.37	0.85	-	0.26
		RMSE	1.88	2.33	8.40	-	6.01
		Bias	**0.00**	**0.00**	**0.02**	-	0.01
		MAE	1.34	1.82	6.34	-	3.09
	EQM	Pearson	0.98	0.37	**0.86**	-	0.26
		RMSE	**1.39**	2.33	8.06	-	5.92
		Bias	0.03	0.01	-0.11	-	-0.03
		MAE	**1.04**	1.82	**6.04**	-	3.06

References

Anderson, B., Mackintosh, A., Stumm, D., George, L., Kerr, T., Winter-Billington, A., and Fitzsimons, S.: Climate sensitivity of a high-precipitation glacier in New Zealand, Journal of Glaciology, 56, 114-128, 2010.

Anslow, F. S., Hostetler, S., Bidlake, W. R., and Clark, P. U.: Distributed energy balance modeling of South Cascade Glacier, Washington and assessment of model uncertainty, Journal of Geophysical Research: Earth Surface, 113, 2008.

Arnold, N., Willis, I., Sharp, M., Richards, K., and Lawson, W.: A distributed surface energy-balance model for a small valley glacier. I. Development and testing for Haut Glacier d'Arolla, Valais, Switzerland, Journal of Glaciology, 42, 77-89, 1996.

Bach, E., Radić, V., and Schoof, C.: How sensitive are mountain glaciers to climate change? Insights from a block model, Journal of Glaciology, 64, 247-258, 2018.

Bamber, J. L., Westaway, R. M., Marzeion, B., and Wouters, B.: The land ice contribution to sea level during the satellite era, Environmental Research Letters, 13, 063008, 2018.

Barnett, T. P., Adam, J. C., and Lettenmaier, D. P.: Potential impacts of a warming climate on water availability in snow-dominated regions, Nature, 438, 303-309, 10.1038/nature04141, 2005.

Bolch, T., Menounos, B., and Wheate, R.: Landsat-based inventory of glaciers in western Canada, 1985-2005, Remote Sensing of Environment, 114, 127-137, 10.1016/j.rse.2009.08.015, 2010.

Bonekamp, P. N., de Kok, R. J., Collier, E., and Immerzeel, W. W.: Contrasting meteorological drivers of the glacier mass balance between the Karakoram and central Himalaya, Frontiers in Earth Science, 7, 107, 2019.

Bordeleau, P.-A.: Modélisation hydrologique de hautes montagnes basée sur un bilan net d'échanges radiatifs calculé à l'aide de la télédétection, Université du Québec à Trois-Rivières, 1998.

Brock, B. W., Willis, I. C., and Sharp, M. J.: Measurement and parameterization of aerodynamic roughness length variations at Haut Glacier d'Arolla, Switzerland, Journal of Glaciology, 52, 281-297, 2006.

Cannon, A. J., Sobie, S. R., and Murdock, T. Q.: Bias correction of GCM precipitation by quantile mapping: How well do methods preserve changes in quantiles and extremes? Journal of Climate, 28, 6938-6959, 2015.

Carenzo, M., Pellicciotti, F., Rimkus, S., and Burlando, P.: Assessing the transferability and robustness of an enhanced temperature-index glacier-melt model, Journal of Glaciology, 55, 258-274, 2009.

Carenzo, M.: Distributed modelling of changes in glacier mass balance and runoff, Diss., Eidgenössische Technische Hochschule ETH Zürich, Nr. 20616, 2012, 2012.

Choi, W., Kim, S. J., Rasmussen, P. F., and Moore, A. R.: Use of the North American Regional Reanalysis for hydrological modelling in Manitoba, Canadian Water Resources Journal, 34, 17-36, 2009.

Clarke, G. K., Jarosch, A. H., Anslow, F. S., Radić, V., and Menounos, B.: Projected deglaciation of western Canada in the twenty-first century, Nature Geoscience, 2015.

Cogley, J. G., and Adams, W.: Mass balance of glaciers other than the ice sheets, Journal of Glaciology, 44, 315-325, 1998.

Comeau, L. E., Pietroniro, A., and Demuth, M. N.: Glacier contribution to the North and South Saskatchewan rivers, Hydrological Processes, 23, 2640-2653, 2009.

Cuffey, K. M., and Paterson, W. S. B.: The physics of glaciers, 4th ed. ed., Butterworth-Heinemann/Elsevier, Burlington, Mass., xii, 693 p, 2010.

Dadic, R., Mott, R., Lehning, M., and Burlando, P.: Wind influence on snow depth distribution and accumulation over glaciers, Journal of Geophysical Research: Earth Surface, 115, 2010.

De Woul, M., and Hock, R.: Static mass-balance sensitivity of Arctic glaciers and ice caps using a degree-day approach, Annals of Glaciology, 42, 217-224, 2005.

Demuth, M., and Pietroniro, A.: Inferring glacier mass balance using RADARSAT: results from Peyto Glacier, Canada, Geografiska Annaler: Series A, Physical Geography, 81, 521-540, 1999.

Demuth, M., and Pietroniro, A.: The impact of climate change on the glaciers of the Canadian Rocky Mountain eastern slopes and implications for water resource-related adaptation in the Canadian prairies, Phase I"-Headwaters of the North Saskatchewan River Basin. GSC Open File, 4322, 2003.

Demuth, M., Munro, D. S., and Young, G. J.: Peyto Glacier: one century of science, Environment Canada, 2006.

Déry, S. J., Stahl, K., Moore, R., Whitfield, P., Menounos, B., and Burford, J. E.: Detection of runoff timing changes in pluvial, nival, and glacial rivers of western Canada, Water Resources Research, 45, 2009.

DeWalle, D. R., and Rango, A.: Principles of snow hydrology, Cambridge University Press, 2008.

Dittmer, K.: Changing streamflow on Columbia basin tribal lands–climate change and salmon, Climatic Change, 120, 627-641, 2013.

Ebrahimi, S., and Marshall, S. J.: Surface energy balance sensitivity to meteorological variability on Haig Glacier, Canadian Rocky Mountains, The Cryosphere, 10, 2799-2819, 2016.

Erler, A. R., Peltier, W. R., and d'Orgeville, M.: Dynamically downscaled high-resolution hydroclimate projections for western Canada, Journal of Climate, 28, 423-450, 2015.

Essou, G. R. C., Sabarly, F., Lucas-Picher, P., Brissette, F., and Poulin, A.: Can Precipitation and Temperature from Meteorological Reanalyses Be Used for Hydrological Modeling? Journal of Hydrometeorology, 17, 1929-1950, 10.1175/jhm-d-15-0138.1, 2016.

Fassnacht, S.: Estimating Alter-shielded gauge snowfall undercatch, snowpack sublimation, and blowing snow transport at six sites in the coterminous USA, Hydrological Processes, 18, 3481-3492, 2004.

Fountain, A. G., and Tangborn, W. V.: The effect of glaciers on streamflow variations, Water Resources Research, 21, 579-586, 1985.

Gabbi, J., Carenzo, M., Pellicciotti, F., Bauder, A., and Funk, M.: A comparison of empirical and physically based glacier surface melt models for long-term simulations of glacier response, Journal of Glaciology, 60, 1140-1154, 10.3189/2014JoG14J011, 2014.

Gardner, A. S., Moholdt, G., Cogley, J. G., Wouters, B., Arendt, A. A., Wahr, J., Berthier, E., Hock, R., Pfeffer, W. T., and Kaser, G.: A reconciled estimate of glacier contributions to sea level rise: 2003 to 2009, science, 340, 852-857, 2013.

Gerbaux, M., Genthon, C., Etchevers, P., Vincent, C., and Dedieu, J.: Surface mass balance of glaciers in the French Alps: distributed modeling and sensitivity to climate change, Journal of Glaciology, 51, 561-572, 2005.

Grah, O., and Beaulieu, J.: The effect of climate change on glacier ablation and baseflow support in the Nooksack River basin and implications on Pacific salmonid species protection and recovery, Climatic Change, 120, 657-670, 2013.

Gratton, D. J., Howarth, P. J., and Marceau, D. J.: Using Landsat-5 Thematic Mapper and digital elevation data to determine the net radiation field of a mountain glacier, Remote Sensing of Environment, 43, 315-331, 1993.

Heusser, C. J.: Postglacial environments in the Canadian Rocky mountains, Ecological Monographs, 26, 263-302, 1956.

Hock, R., and Holmgren, B.: Some aspects of energy balance and ablation of Storglaciären, northern Sweden, Geografiska Annaler: Series A, Physical Geography, 78, 121-131, 1996.

Hock, R.: A distributed temperature-index ice-and snowmelt model including potential direct solar radiation, Journal of Glaciology, 45, 101-111, 1999.

Hock, R.: Temperature index melt modelling in mountain areas, Journal of Hydrology, 282, 104-115, 2003.

Hock, R., and Holmgren, B.: A distributed surface energy-balance model for complex topography and its application to Storglaciären, Sweden, Journal of Glaciology, 51, 25-36, 2005.

Hock, R., Jansson, P., and Braun, L. N.: Modelling the Response of Mountain Glacier Discharge to Climate Warming, 23, 243-252, 10.1007/1-4020-3508-x_25, 2005.

Hofer, M., Mölg, T., Marzeion, B., and Kaser, G.: Empirical-statistical downscaling of reanalysis data to high-resolution air temperature and specific humidity above a glacier surface (Cordillera Blanca, Peru), Journal of Geophysical Research: Atmospheres, 115, 2010.

Hofer, M., Nemec, J., Cullen, N. J., and Weber, M.: Evaluating predictor strategies for regression-based downscaling with a focus on glacierized mountain environments, Journal of Applied Meteorology and Climatology, 56, 1707-1729, 10.1175/jamc-d-16-0215.1, 2017.

Huss, M., Hock, R., Bauder, A., and Funk, M.: Conventional versus reference-surface mass balance, Journal of Glaciology, 58, 278-286, 2012.

Huss, M., Bookhagen, B., Huggel, C., Jacobsen, D., Bradley, R. S., Clague, J. J., Vuille, M., Buytaert, W., Cayan, D. R., and Greenwood, G.: Toward mountains without permanent snow and ice, Earth's Future, 5, 418-435, 2017.

IPCC: Managing the Risks of Extreme Events and Disasters to Advance Climate Change Adaptation. A Special Report of Working Groups I and II of the Intergovernmental Panel on Climate Change, Cambridge University Press, Cambridge, United Kingdom, and New York, NY, USA, 582 pp., 2012.

Jacob, T., Wahr, J., Pfeffer, W. T., and Swenson, S.: Recent contributions of glaciers and ice caps to sea level rise, Nature, 482, 514-518, 2012.

Jansson, P., Hock, R., and Schneider, T.: The concept of glacier storage: a review, Journal of Hydrology, 282, 116-129, 2003.

Jennings, K. S., Winchell, T. S., Livneh, B., and Molotch, N. P.: Spatial variation of the rain–snow temperature threshold across the Northern Hemisphere, Nature communications, 9, 1-9, 2018.

Keshta, N., and Elshorbagy, A.: Utilizing North American regional reanalysis for modeling soil moisture and evapotranspiration in reconstructed watersheds, Physics and Chemistry of the Earth, Parts A/B/C, 36, 31-41, 2011.

Kim, Y., Hatsushika, H., Muskett, R. R., and Yamazaki, K.: Possible effect of boreal wildfire soot on Arctic sea ice and Alaska glaciers, Atmospheric Environment, 39, 3513-3520, 2005.

Klok, E., and Oerlemans, J.: Model study of the spatial distribution of the energy and mass balance of Morteratschgletscher, Switzerland, Journal of Glaciology, 48, 505-518, 2002.

Konzelmann, T., van de Wal, R. S., Greuell, W., Bintanja, R., Henneken, E. A., and Abe-Ouchi, A.: Parameterization of global and longwave incoming radiation for the Greenland Ice Sheet, Global and Planetary change, 9, 143-164, 1994.

Lutz, S., Anesio, A. M., Jorge Villar, S. E., and Benning, L. G.: Variations of algal communities cause darkening of a Greenland glacier, FEMS Microbiology Ecology, 89, 402-414, 2014.

MacDougall, A. H., and Flowers, G. E.: Spatial and temporal transferability of a distributed energy-balance glacier melt model, Journal of Climate, 24, 1480-1498, 2011.

Marshall, S. J., White, E. C., Demuth, M. N., Bolch, T., Wheate, R., Menounos, B., Beedle, M. J., and Shea, J. M.: Glacier water resources on the eastern slopes of the Canadian Rocky Mountains, Canadian Water Resources Journal, 36, 109-134, 2011.

Mattar, K. E., Vachon, P. W., Geudtner, D., Gray, A. L., Cumming, I. G., and Brugman, M.: Validation of alpine glacier velocity measurements using ERS tandem-mission SAR data, IEEE Transactions on Geoscience and Remote Sensing, 36, 974-984, 1998.

Matthews, T., Hodgkins, R., Wilby, R. L., Guðmundsson, S., Pálsson, F., Björnsson, H., and Carr, S.: Conditioning temperature-index model parameters on synoptic weather types for glacier melt simulations, Hydrological Processes, 29, 1027-1045, 2015.

Meier, M. F.: Mode of flow of Saskatchewan Glacier, Alberta, Canada, US Govt. Print. Off.2330-7102, 1960.

Meier, M. F., Dyurgerov, M. B., Rick, U. K., O'Neel, S., Pfeffer, W. T., Anderson, R. S., Anderson, S. P., and Glazovsky, A. F.: Glaciers dominate eustatic sea-level rise in the 21st century, Science, 317, 1064-1067, 2007.

Mesinger, F., DiMego, G., Kalnay, E., Mitchell, K., Shafran, P. C., Ebisuzaki, W., Jović, D., Woollen, J., Rogers, E., and Berbery, E. H.: North American regional reanalysis, Bulletin of the American Meteorological Society, 87, 343-360, 2006.

Milner, A. M., Khamis, K., Battin, T. J., Brittain, J. E., Barrand, N. E., Füreder, L., Cauvy-Fraunié, S., Gíslason, G. M., Jacobsen, D., and Hannah, D. M.: Glacier shrinkage driving global changes in downstream systems, Proceedings of the National Academy of Sciences, 114, 9770-9778, 2017.

Mölg, T., Cullen, N. J., Hardy, D. R., Kaser, G., and Klok, L.: Mass balance of a slope glacier on Kilimanjaro and its sensitivity to climate, International Journal of Climatology: A Journal of the Royal Meteorological Society, 28, 881-892, 2008.

Mölg, T., Großhauser, M., Hemp, A., Hofer, M., and Marzeion, B.: Limited forcing of glacier loss through land-cover change on Kilimanjaro, Nature Climate Change, 2, 254, 2012.

Munro, D. S.: Surface roughness and bulk heat transfer on a glacier: comparison with eddy correlation, Journal of Glaciology, 35, 343-348, 1989.

Nakawo, M., and Young, G. J.: Field experiments to determine the effect of a debris layer on ablation of glacier ice, Annals of Glaciology, 2, 85-91, 1981.

Nash, J. E., and Sutcliffe, J. V.: River flow forecasting through conceptual models part I–A discussion of principles, Journal of hydrology, 10, 282-290, 1970.

Nicholls, R. J., and Cazenave, A.: Sea-level rise and its impact on coastal zones, science, 328, 1517-1520, 2010.

Oerlemans, J., and Fortuin, J.: Sensitivity of glaciers and small ice caps to greenhouse warming, Science, 258, 115-117, 1992.

Oerlemans, J.: Quantifying global warming from the retreat of glaciers, Science-AAAS-Weekly Paper Edition-including Guide to Scientific Information, 264, 243-244, 1994.

Oerlemans, J., Anderson, B., Hubbard, A., Huybrechts, P., Johannesson, T., Knap, W., Schmeits, M., Stroeven, A., Van de Wal, R., and Wallinga, J.: Modelling the response of glaciers to climate warming, Climate dynamics, 14, 267-274, 1998.

Oerlemans, J., and Knap, W.: A 1 year record of global radiation and albedo in the ablation zone of Morteratschgletscher, Switzerland, Journal of Glaciology, 44, 231-238, 1998.

Oerlemans, J.: Glaciers and climate change, CRC Press, 2001.

Oerlemans, J., Giesen, R., and Van den Broeke, M.: Retreating alpine glaciers: increased melt rates due to accumulation of dust (Vadret da Morteratsch, Switzerland), Journal of Glaciology, 55, 729-736, 2009.

Oke, T.: Boundary layer climates0415043190, 1987.

Østby, T. I., Schuler, T., Hagen, J. O. M., Hock, R., Kohler, J., and Reijmer, C.: Diagnosing the decline in climatic mass balance of glaciers in Svalbard over 1957-2014, The Cryosphere, 11, 191-215, 2017.

Pellicciotti, F., Brock, B., Strasser, U., Burlando, P., Funk, M., and Corripio, J.: An enhanced temperature-index glacier melt model including the shortwave radiation balance: development and testing for Haut Glacier d'Arolla, Switzerland, Journal of Glaciology, 51, 573-587, 2005.

Petersen, L., and Pellicciotti, F.: Spatial and temporal variability of air temperature on a melting glacier: atmospheric controls, extrapolation methods and their effect on melt modeling, Juncal Norte Glacier, Chile, Journal of Geophysical Research: Atmospheres, 116, 2011.

Pollock, E. W., and Bush, A. B.: Changes in snow mass balance in the Canadian Rocky Mountains caused by CO2 rise: Regional atmosphere model results, Atmosphere-Ocean, 51, 505-521, 2013.

Prudhomme, C., Wilby, R. L., Crooks, S., Kay, A. L., and Reynard, N. S.: Scenario-neutral approach to climate change impact studies: application to flood risk, Journal of Hydrology, 390, 198-209, 2010.

Radic, V., Tessema, M., Menounos, B., and Fitzpatrick, N.: Evaluation of Dynamically Downscaled Near-surface Mass and Energy Fluxes for Three Mountain Glaciers, British Columbia, Canada, AGU Fall Meeting Abstracts, 2018,

Radić, V., and Hock, R.: Modeling future glacier mass balance and volume changes using ERA-40 reanalysis and climate models: A sensitivity study at Storglaciären, Sweden, Journal of Geophysical Research: Earth Surface, 111, 2006.

Radić, V., and Hock, R.: Regionally differentiated contribution of mountain glaciers and ice caps to future sea-level rise, Nature Geoscience, 4, 91-94, 2011.

Rasmussen, R., Liu, C., Ikeda, K., Gochis, D., Yates, D., Chen, F., Tewari, M., Barlage, M., Dudhia, J., and Yu, W.: High-resolution coupled climate runoff simulations of seasonal snowfall over Colorado: a process study of current and warmer climate, Journal of Climate, 24, 3015-3048, 2011.

Rasmussen, R., Baker, B., Kochendorfer, J., Meyers, T., Landolt, S., Fischer, A. P., Black, J., Thériault, J. M., Kucera, P., and Gochis, D.: How well are we measuring snow: The NOAA/FAA/NCAR winter precipitation test bed, Bulletin of the American Meteorological Society, 93, 811-829, 2012.

Refsgaard, J. C., Madsen, H., Andréassian, V., Arnbjerg-Nielsen, K., Davidson, T., Drews, M., Hamilton, D., Jeppesen, E., Kjellström, E., and Olesen, J.: A framework for testing the ability of models to project climate change and its impacts, Climatic change, 122, 271-282, 2014.

Réveillet, M., Six, D., Vincent, C., Rabatel, A., Dumont, M., Lafaysse, M., Morin, S., Vionnet, V., and Litt, M.: Relative performance of empirical and physical models in assessing seasonal and annual glacier surface mass balance in the French Alps, 2017a.

Réveillet, M., Vincent, C., Six, D., and Rabatel, A.: Which empirical model is best suited to simulate glacier mass balances? Journal of Glaciology, 63, 39-54, 2017b.

Rye, C. J., Arnold, N. S., Willis, I. C., and Kohler, J.: Modeling the surface mass balance of a high Arctic glacier using the ERA-40 reanalysis, Journal of Geophysical Research: Earth Surface, 115, 2010.

Schindler, D. W., and Donahue, W. F.: An impending water crisis in Canada's western prairie provinces, Proceedings of the National Academy of Sciences, 103, 7210-7216, 2006.

Takeuchi, N., Kohshima, S., and Seko, K.: Structure, formation, and darkening process of albedo-reducing material (cryoconite) on a Himalayan glacier: a granular algal mat growing on the glacier, Arctic, Antarctic, and Alpine Research, 33, 115-122, 2001.

Tennant, C., Menounos, B., Wheate, R., and Clague, J.: Area change of glaciers in the Canadian Rocky Mountains, 1919 to 2006, The Cryosphere, 6, 1541-1552, 2012.

Tennant, C., and Menounos, B.: Glacier change of the Columbia Icefield, Canadian Rocky Mountains, 1919-2009, Journal of Glaciology, 59, 671-686, 2013.

Thibert, E., Blanc, R., Vincent, C., and Eckert, N.: Glaciological and volumetric mass-balance measurements: error analysis over 51 years for Glacier de Sarennes, French Alps, Journal of Glaciology, 54, 522-532, 2008.

Trouet, V., and Van Oldenborgh, G. J.: KNMI Climate Explorer: a web-based research tool for high-resolution paleoclimatology, Tree-Ring Research, 69, 3-14, 2013.

Van den Hurk, B., Tank, A. K., Lenderink, G., van Ulden, A., van Oldenborgh, G. J., Katsman, C., van den Brink, H., Keller, F., Bessembinder, J., and Burgers, G.: New climate change scenarios for the Netherlands, Water science and technology, 56, 27-33, 2007.

Wang, Z., Erb, A. M., Schaaf, C. B., Sun, Q., Liu, Y., Yang, Y., Shuai, Y., Casey, K. A., and Román, M. O.: Early spring post-fire snow albedo dynamics in high latitude boreal forests using Landsat-8 OLI data, Remote sensing of environment, 185, 71-83, 2016.

Wetterhall, F., Pappenberger, F., He, Y., Freer, J., and Cloke, H. L.: Conditioning model output statistics of regional climate model precipitation on circulation patterns, Nonlinear Processes in Geophysics, 19, 623-633, 10.5194/npg-19-623-2012, 2012.

Wheler, B. A.: Glacier melt modelling in the Donjek Range, St. Elias Mountains, Yukon Territory, Dept. of Earth Sciences-Simon Fraser University, 2009.

Zemp, M., Thibert, E., Huss, M., Stumm, D., Denby, C. R., Nuth, C., Nussbaumer, S., Moholdt, G., Mercer, A., and Mayer, C.: Uncertainties and re-analysis of glacier mass balance measurements, The Cryosphere Discussions, 7, 789-839, 2013.

Zemp, M., Frey, H., Gärtner-Roer, I., Nussbaumer, S. U., Hoelzle, M., Paul, F., Haeberli, W., Denzinger, F., Ahlstrøm, A. P., and Anderson, B.: Historically unprecedented global glacier decline in the early 21st century, Journal of Glaciology, 61, 745-762, 2015.

Zemp, M., Nussbaumer, S. U., Gärtner-Roer, I., Huber, J., Machguth, H., Paul, F., and Hoelzle, M.: Global Glacier Change Bulletin No. 2 (2014-2015), Global Glacier Change Bulletin, 2, 2017.

CHAPITRE III

CONCLUSION GÉNÉRALE

L'objectif principal de ce projet était d'étudier l'impact de la structure des modèles glaciologiques à base empirique de différentes complexités sur la capacité de ces modèles à simuler le bilan de masse glaciologique dans un climat futur en les comparant au bilan de masse de référence calculé par le modèle physique sur le glacier Saskatchewan. Vu l'envergure du projet à la suite de la présentation de celui-ci, nous avons révisé nos objectifs et concentré nos efforts sur la modélisation et l'analyse en détails du bilan de masse de référence avec l'utilisation d'un modèle à base physique. À la lumière de ces nouveaux résultats, toutes nos hypothèses ont été confirmées, ce qui a permis d'en tirer les conclusions suivantes :

1) La comparaison de certaines variables des réanalyses climatiques NARR avec les observations AWS ont offert une bonne performance avant la mise à l'échelle : Ta ($R = 0.98$), SWin ($R = 0.92$), RH ($R = 0.85$). La mise à l'échelle simple (Scaling) vers la station AWS a été utilisée pour tous les variables excepté RH. Cette méthode a offert une correction du biais pour les erreurs reliées entre autres à la différence d'altitude et autres erreurs structurelles du modèle NARR. La variable WS et P ne concordent pas avec les observations ($R = 0.37$ et 0.30). Les vents très locaux du glacier ont une dynamique différente des vents simulés par le NARR, davantage en altitude. Les précipitations sont connues pour être des variables difficiles à bien simuler et extrapoler. Le biais entre les NARR (2430 m) et la série de précipitation homogénéisé avec deux stations (~2002 m) ne peut pas être complètement expliqué par la différence d'altitude. Un facteur de correction (PCF) de 10 % a été utilisé après la mise à l'échelle pour combler la sous-estimation typique des précipitations neigeuses des stations météorologiques. En général, les données météorologiques sont satisfaisantes pour forcer le modèle de bilan de masse

glaciaire à base physique considérant le peu d'observation disponible près du glacier Saskatchewan (Table 1 – Chapitre II).

2) Le bilan de masse simulé par le modèle à base physique correspond bien aux observations de bilan de masse glaciologique de 2012 à 2016. Le bilan hivernal (bw) contient plus d'observation et atteint un NSE de 0,71 alors que le bilan annuel (ba) atteint une valeur de NSE de 0,94 (Fig. 6 – Chapitre II).

3) La reconstruction du bilan de masse historique forcé par les données climatiques NARR mise à l'échelle se situe aux limites des marges d'erreur du bilan de masse géodésique calculé par Tennant et Menounos (2013). La marge d'erreur de ce dernier pourrait être réduite en soustrayant le DEM 1979 au DEM de 2009 directement au lieu d'accumuler l'erreur à chaque soustraction (Fig. 8 – Chapitre II). Les variations du Ba glaciologique du glacier Peyto et du Ba reconstruit du glacier Saskatchewan sont relativement synchrones ($R = 0.56$), mais inférieures aux prévisions théoriques étant donné la courte distance de séparation de 70 km (Fig. 9 – Chapitre II).

4) L'impact du retrait glaciaire sur le bilan de masse est faible (~ ±1.4 m w.e. sur 37 ans) puisque la topographie du front du glacier de 1979 et 2009 se situe dans le creux de la vallée à la même altitude. Cela limite une rétroaction négative du retrait glaciaire sur le bilan de masse. Ainsi, il y aura une réduction de la fonte en raison des températures plus basses lorsque le glacier se retirera à des altitudes plus élevées (Fig. 8 – Chapitre II).

5) Nous avons procédé à l'analyse détaillée du bilan d'énergie et de la sensibilité du bilan de masse aux changements de températures et de précipitations dans un avenir à moyen (2046-2065) et long terme (2081-2100). Les conclusions permettent d'affirmer que l'augmentation possible de 20 % des précipitations n'est pas suffisante pour contrer la fonte de Ba dû à l'augmentation de la température de l'air. Nous avons calculé une mesure de Ba de -0.49 cm w.e. par année sur la période de référence de 1981 à 2000. Cette mesure a été comparée avec d'autres simulations faisant varier la température de l'air entre

0 et 8 °C et les précipitations entre 0 et +20 %. Sous le scénario RCP +6.0, Ba pourrait encore diminuer de -1.2 m w.e. par année à moyen terme et -2 m w.e. par année à long terme (Fig. 14 – Chapitre II).

3.1 Perspectives futures

L'objectif initial de l'analyse des erreurs structurelles des modèles glaciologiques à base empirique de différentes complexités sur la capacité de ces modèles à simuler le bilan de masse glaciologique dans un climat futur sera repris dans d'éventuels travaux. La base de données initiée dans ce mémoire permettra un premier pas vers cette analyse rigoureuse qui nécessite un bilan de masse de référence simulé par un modèle physique ainsi que ses données météorologiques et topographiques. Quelques ajustements au niveau de la calibration et des DEM seront apportés avec de nouvelles observations glaciologiques, mais une première analyse exploratoire serait intéressante. Suite à ces travaux sur l'analyse des modèles empiriques, il est espéré que la méthode développée et testée sur le glacier Saskatchewan sera applicable à d'autres glaciers dans le monde.

RÉFÉRENCES BIBLIOGRAPHIQUES

Barnett, T. P., Adam, J. C., and Lettenmaier, D. P.: Potential impacts of a warming climate on water availability in snow-dominated regions, Nature, 438, 303-309, 10.1038/nature04141, 2005.

Barry, R. G.: The status of research on glaciers and global glacier recession: a review, Progress in Physical Geography, 30, 285-306, 2006.

Beniston, M.: Climatic change in mountain regions: a review of possible impacts, in: Climate variability and change in high elevation regions: Past, present & future, Springer, 5-31, 2003.

Benn, D. I., and Evans, D. J. A.: Glaciers & glaciation, Second edition. ed., Glaciers et glaciation, Routledge, Taylor & Francis Group, London, xiv, 802 pp., 2010.

Bolch, T., Menounos, B., and Wheate, R.: Landsat-based inventory of glaciers in western Canada, 1985-2005, Remote Sensing of Environment, 114, 127-137, 10.1016/j.rse.2009.08.015, 2010.

Bonekamp, P. N., de Kok, R. J., Collier, E., and Immerzeel, W. W.: Contrasting meteorological drivers of the glacier mass balance between the Karakoram and central Himalaya, Frontiers in Earth Science, 7, 107, 2019.

Carenzo, M., Pellicciotti, F., Rimkus, S., and Burlando, P.: Assessing the transferability and robustness of an enhanced temperature-index glacier-melt model, Journal of Glaciology, 55, 258-274, 2009.

Carenzo, M.: Distributed modelling of changes in glacier mass balance and runoff, Diss., Eidgenössische Technische Hochschule ETH Zürich, Nr. 20616, 2012, 2012.

Clarke, G. K., Jarosch, A. H., Anslow, F. S., Radić, V., and Menounos, B.: Projected deglaciation of western Canada in the twenty-first century, Nature Geoscience, 2015.

Comeau, L. E., Pietroniro, A., and Demuth, M. N.: Glacier contribution to the North and South Saskatchewan rivers, Hydrological Processes, 23, 2640-2653, 2009.

Cuffey, K. M., and Paterson, W. S. B.: The physics of glaciers, 4th ed. ed., Butterworth-Heinemann/Elsevier, Burlington, Mass., xii, 693 pp., 2010.

Dittmer, K.: Changing streamflow on Columbia basin tribal lands–climate change and salmon, Climatic Change, 120, 627-641, 2013.

Gabbi, J., Carenzo, M., Pellicciotti, F., Bauder, A., and Funk, M.: A comparison of empirical and physically based glacier surface melt models for long-term simulations of glacier response, Journal of Glaciology, 60, 1140-1154, 10.3189/2014JoG14J011, 2014.

Giesen, R. H., and Oerlemans, J.: Climate-model induced differences in the 21st century global and regional glacier contributions to sea-level rise, Climate dynamics, 41, 3283-3300, 2013.

Grah, O., and Beaulieu, J.: The effect of climate change on glacier ablation and baseflow support in the Nooksack River basin and implications on Pacific salmonid species protection and recovery, Climatic Change, 120, 657-670, 2013.

Hock, R.: A distributed temperature-index ice-and snowmelt model including potential direct solar radiation, Journal of Glaciology, 45, 101-111, 1999.

Hock, R.: Temperature index melt modelling in mountain areas, Journal of Hydrology, 282, 104-115, 2003.

Hock, R., and Holmgren, B.: A distributed surface energy-balance model for complex topography and its application to Storglaciären, Sweden, Journal of Glaciology, 51, 25-36, 2005.

Hock, R., and Radić, V.: Climate sensitivity of Storglaciären, Sweden: an intercomparison of mass-balance models using ERA-40 re-analysis and regional climate model data, Annals of glaciology, 46, 342-348, 2007.

Hofer, M., Mölg, T., Marzeion, B., and Kaser, G.: Empirical-statistical downscaling of reanalysis data to high-resolution air temperature and specific humidity above a glacier surface (Cordillera Blanca, Peru), Journal of Geophysical Research: Atmospheres, 115, 2010.

Huss, M., Farinotti, D., Bauder, A., and Funk, M.: Modelling runoff from highly glacierized alpine drainage basins in a changing climate, Hydrological processes, 22, 3888-3902, 2008.

Huss, M., Zemp, M., Joerg, P. C., and Salzmann, N.: High uncertainty in 21st century runoff projections from glacierized basins, Journal of Hydrology, 510, 35-48, 2014.

Immerzeel, W., Pellicciotti, F., and Bierkens, M.: Rising river flows throughout the twenty-first century in two Himalayan glacierized watersheds, Nature Geoscience, 6, 742-745, 2013.

Jacob, T., Wahr, J., Pfeffer, W. T., and Swenson, S.: Recent contributions of glaciers and ice caps to sea level rise, Nature, 482, 514-518, 2012.

Jansson, P., Hock, R., and Schneider, T.: The concept of glacier storage: a review, Journal of Hydrology, 282, 116-129, 2003.

Kapos, V., Rhind, J., Edwards, M., Price, M., Ravilious, C., and Butt, N.: Developing a map of the world's mountain forests, Forests in sustainable mountain development: a state of knowledge report for 2000. Task Force on Forests in Sustainable Mountain Development., 4-19, 2000.

Kaser, G.: A review of the modern fluctuations of tropical glaciers, Global and Planetary Change, 22, 93-103, 1999.

MacDougall, A. H., and Flowers, G. E.: Spatial and temporal transferability of a distributed energy-balance glacier melt model, Journal of Climate, 24, 1480-1498, 2011.

Marshall, S. J., White, E. C., Demuth, M. N., Bolch, T., Wheate, R., Menounos, B., Beedle, M. J., and Shea, J. M.: Glacier water resources on the eastern slopes of the Canadian Rocky Mountains, Canadian Water Resources Journal, 36, 109-134, 2011.

Marzeion, B., Jarosch, A., and Hofer, M.: Past and future sea-level change from the surface mass balance of glaciers, The Cryosphere, 6, 1295-1322, 2012.

Matthews, J. A., and Briffa, K. R.: The 'Little Ice Age': Re-evaluation of an evolving concept, Geografiska Annaler: Series A, Physical Geography, 87, 17-36, 2005.

Matthews, T., Hodgkins, R., Wilby, R. L., Guðmundsson, S., Pálsson, F., Björnsson, H., and Carr, S.: Conditioning temperature-index model parameters on synoptic weather types for glacier melt simulations, Hydrological Processes, 29, 1027-1045, 2015.

Meier, M. F., Dyurgerov, M. B., Rick, U. K., O'Neel, S., Pfeffer, W. T., Anderson, R. S., Anderson, S. P., and Glazovsky, A. F.: Glaciers dominate eustatic sea-level rise in the 21st century, Science, 317, 1064-1067, 2007.

Mesinger, F., DiMego, G., Kalnay, E., Mitchell, K., Shafran, P. C., Ebisuzaki, W., Jović, D., Woollen, J., Rogers, E., and Berbery, E. H.: North American regional reanalysis, Bulletin of the American Meteorological Society, 87, 343-360, 2006.

Meybeck, M., Green, P., and Vörösmarty, C.: A new typology for mountains and other relief classes: an application to global continental water resources and population distribution, Mountain Research and Development, 21, 34-45, 2001.

Mölg, T., Großhauser, M., Hemp, A., Hofer, M., and Marzeion, B.: Limited forcing of glacier loss through land-cover change on Kilimanjaro, Nature Climate Change, 2, 254, 2012.

Nicholls, R. J., and Cazenave, A.: Sea-level rise and its impact on coastal zones, science, 328, 1517-1520, 2010.

Oerlemans, J.: Quantifying global warming from the retreat of glaciers, Science-AAAS-Weekly Paper Edition-including Guide to Scientific Information, 264, 243-244, 1994.

Østby, T. I., Schuler, T., Hagen, J. O. M., Hock, R., Kohler, J., and Reijmer, C.: Diagnosing the decline in climatic mass balance of glaciers in Svalbard over 1957-2014, The Cryosphere, 11, 191-215, 2017.

Pellicciotti, F., Brock, B., Strasser, U., Burlando, P., Funk, M., and Corripio, J.: An enhanced temperature-index glacier melt model including the shortwave radiation balance: development and testing for Haut Glacier d'Arolla, Switzerland, Journal of Glaciology, 51, 573-587, 2005.

Radic, V., Tessema, M., Menounos, B., and Fitzpatrick, N.: Evaluation of Dynamically Downscaled Near-surface Mass and Energy Fluxes for Three Mountain Glaciers, British Columbia, Canada, AGU Fall Meeting Abstracts, 2018.

Radić, V., and Hock, R.: Modeling future glacier mass balance and volume changes using ERA-40 reanalysis and climate models: A sensitivity study at Storglaciären, Sweden, Journal of Geophysical Research: Earth Surface, 111, 2006.

Radić, V., Bliss, A., Beedlow, A. C., Hock, R., Miles, E., and Cogley, J. G.: Regional and global projections of twenty-first century glacier mass changes in response to climate scenarios from global climate models, Climate Dynamics, 42, 37-58, 2014.

Raper, S. C., and Braithwaite, R. J.: Low sea level rise projections from mountain glaciers and icecaps under global warming, Nature, 439, 311-313, 2006.

Refsgaard, J. C., Madsen, H., Andréassian, V., Arnbjerg-Nielsen, K., Davidson, T., Drews, M., Hamilton, D., Jeppesen, E., Kjellström, E., and Olesen, J.: A framework for testing the ability of models to project climate change and its impacts, Climatic change, 122, 271-282, 2014.

Schindler, D. W., and Donahue, W. F.: An impending water crisis in Canada's western prairie provinces, Proceedings of the National Academy of Sciences, 103, 7210-7216, 2006.

Shiklomanov, I. A.: World water resources, A new appraisal and assessment for the 21st century, 1998.

Tennant, C., Menounos, B., Wheate, R., and Clague, J.: Area change of glaciers in the Canadian Rocky Mountains, 1919 to 2006, The Cryosphere, 6, 1541-1552, 2012.

Tennant, C., and Menounos, B.: Glacier change of the Columbia Icefield, Canadian Rocky Mountains, 1919–2009, Journal of Glaciology, 59, 671-686, 2013.

Wheler, B. A.: Glacier melt modelling in the Donjek Range, St. Elias Mountains, Yukon Territory, Dept. of Earth Sciences-Simon Fraser University, 2009.

Zemp, M., Frey, H., Gärtner-Roer, I., Nussbaumer, S. U., Hoelzle, M., Paul, F., Haeberli, W., Denzinger, F., Ahlstrøm, A. P., and Anderson, B.: Historically unprecedented global glacier decline in the early 21st century, Journal of Glaciology, 61, 745-762, 2015.